

LPM-00-15  
May, 2000

# On the Thermodynamic Bethe Ansatz Equation in Sinh-Gordon Model

Al.Zamolodchikov<sup>1</sup>

Laboratoire de Physique Mathématique<sup>2</sup>  
Université Montpellier II  
Pl.E.Bataillon, 34095 Montpellier, France

## Abstract

Two implicit periodic structures in the solution of sinh-Gordon thermodynamic Bethe ansatz equation are considered. The analytic structure of the solution as a function of complex  $\theta$  is studied to some extent both analytically and numerically. The results make a hint how the CFT integrable structures can be relevant in the sinh-Gordon and staircase models. More motivations are figured out for subsequent studies of the massless sinh-Gordon (i.e. Liouville) TBA equation.

## 1. Sinh-Gordon model

It seems that from the recent developments of the string theory there are some persistent requests about better understanding of the two-dimensional sigma-models with non-compact (in particular singular) target spaces. Physical properties of such models are expected to be quite different from these of the better studied compact sigma-models. It is therefore a challenge for the two-dimensional integrable field theory community to reveal the corresponding peculiarities and new features.

The two-dimensional sinh-Gordon model (ShG) is defined by the (Euclidean) action

$$A_{\text{ShG}} = \int \left[ \frac{1}{4\pi} (\partial_a \phi)^2 + 2\mu \cosh(2b\phi) \right] d^2 x \quad (1.1)$$

I believe that this model can be considered to say as “a model” of (suitably perturbed) non-compact sigma-models, in the sense that its properties are considerably different from

---

<sup>1</sup>On leave of absence from Institute of Theoretical and Experimental Physics, B.Cheremushkinskaya 25, 117259 Moscow, Russia

<sup>2</sup>Laboratoire Associé au CNRS URA-768

those of the perturbed rational conformal field theories, these differences being sometimes quite similar to these between non-compact and compact sigma-models.

In (1.1)  $\mu$  is a dimensional (of dimension  $\mu \sim [\text{mass}]^{2+2b^2}$ ) coupling constant which determines the scale in the model and  $b$  is the dimensionless ShG parameter. For the beginning I suppose it to be real and non-negative. The case  $b = 0$  turns to be somewhat singular for the subsequent considerations and here the study is restricted to positive values  $0 < b < \infty$  only. It is also convenient to use different parameters

$$Q = b + 1/b \quad (1.2)$$

and

$$p = \frac{b}{Q} = \frac{b^2}{1+b^2} \quad (1.3)$$

instead of  $b$ .

The perturbing operators  $\exp(\pm 2b\phi)$  in (1.1) have negative dimension  $\Delta = -b^2$ . To make the coupling  $\mu$  a strict sense we need to fix a normalization of these operators. Here they are implied to be normal ordered w.r.t. the massless (unperturbed) vacuum in the way that in unperturbed theory

$$\langle e^{2b\varphi(x_1)} \dots e^{2b\varphi(x_n)} e^{-2b\varphi(y_1)} \dots e^{-2b\varphi(y_n)} \rangle_{\mu=0} = \frac{\prod_{i,j} |x_i - y_j|^{4b^2}}{\prod_{i>j} (|x_i - x_j| |y_i - y_j|)^{4b^2}} \quad (1.4)$$

The model is known to be integrable and can be solved for many important characteristics. In particular its factorized scattering theory is known since long [1, 2]. The spectrum consists of only one neutral particle  $B(\theta)$  subject to a factorized scattering with two-particle amplitude

$$S(\theta) = \frac{\sinh \theta - i \sin \pi p}{\sinh \theta + i \sin \pi p} \quad (1.5)$$

With the normalization (1.4) the mass  $m$  of this particle is related to the scale parameter  $\mu$  as [3]

$$\pi \mu \frac{\Gamma(b^2)}{\Gamma(1-b^2)} = [m Z(p)]^{2+2b^2} \quad (1.6)$$

where

$$Z(p) = \frac{1}{8\sqrt{\pi}} p^p (1-p)^{1-p} \Gamma\left(\frac{1-p}{2}\right) \Gamma\left(\frac{p}{2}\right) \quad (1.7)$$

Notice that the scattering theory is invariant under the (weak-strong coupling) duality transformation  $b \rightarrow 1/b$  which brings  $p \rightarrow 1-p$ . This means that the physical content of the model remains unchanged up to the overall mass scale. Since the combination (1.7) is again

invariant under  $p \rightarrow 1 - p$ , the mass scale also remains unchanged if the coupling constant  $\mu$  is simultaneously substituted by the “dual” coupling constant  $\tilde{\mu}$  related to  $\mu$  as follows

$$\left( \pi \mu \frac{\Gamma(b^2)}{\Gamma(1-b^2)} \right)^{1/b} = \left( \pi \tilde{\mu} \frac{\Gamma(1/b^2)}{\Gamma(1-1/b^2)} \right)^b \quad (1.8)$$

Therefore the sinh-Gordon model is completely invariant under duality  $b \rightarrow 1/b$ ;  $\mu \rightarrow \tilde{\mu}$ . Due to this symmetry it is sufficient to consider only the region  $0 < b^2 \leq 1$  or  $0 < p \leq 1/2$ .

The infinite volume bulk vacuum energy of the model is also known exactly [4]. In terms of the particle mass  $m$  it is given by the following apparently self-dual expression

$$\mathcal{E} = \frac{m^2}{8 \sinh \pi p} \quad (1.9)$$

## 2. TBA equation

Contrary to the on-mass-shell data of ShG quoted above, the off-mass-shell characteristics such as the correlation functions (with the exception of the vacuum expectation values of some local fields [5, 6] and their matrix elements between the asymptotic states [7]) are not known exactly.

Some progress can be made for the finite size effects where the problem is reduced to a non-linear integral equation known as the thermodynamic Bethe ansatz (TBA) one. Namely, consider the ground state energy  $E(R)$  of the finite size ShG model placed on a circle of finite circumference  $R$ . In the TBA framework it appears as

$$E(R) = -\frac{m}{2\pi} \int \cosh \theta \log (1 + e^{-\varepsilon(\theta)}) d\theta \quad (2.1)$$

It is convenient to introduce also the  $R$ -dependent effective central charge  $c_{\text{eff}}(R)$  as

$$c_{\text{eff}}(R) = -\frac{6R}{\pi} E(R) \quad (2.2)$$

In (2.1)  $\varepsilon(\theta)$  is the solution of the TBA equation

$$mR \cosh \theta = \varepsilon + \varphi * \log (1 + e^{-\varepsilon(\theta)}) \quad (2.3)$$

where  $*$  denotes the  $\theta$ -convolution. The kernel  $\varphi(\theta)$  is related to the ShG scattering data (1.5)

$$\varphi(\theta) = -\frac{i}{2\pi} \frac{d}{d\theta} \log S(\theta) = \frac{1}{2\pi} \frac{4 \sin \pi p \cosh \theta}{\cosh 2\theta - \cos 2\pi p} \quad (2.4)$$

The Fourier transform of the kernel reads

$$\varphi(\omega) = \int e^{i\omega\theta} \varphi(\theta) d\theta = \frac{\cosh \frac{a\pi\omega}{2}}{\cosh \frac{\pi\omega}{2}} \quad (2.5)$$

where the parameter

$$a = 1 - 2p \quad (2.6)$$

is simply reflected  $a \rightarrow -a$  under the duality  $p \rightarrow 1 - p$  and therefore can be taken non-negative  $0 \leq a < 1$ .

The following conclusion are readily made from the structure of the integral equation (2.3).

**1.** Function is even  $\varepsilon(\theta) = \varepsilon(-\theta)$  and analytic in the strip  $|\text{Im } \theta| < \pi/2 - \pi a/2$ . At  $\text{Re } \theta \rightarrow \infty$  in this strip it has the asymptotic  $\varepsilon(\theta) \sim m R e^\theta / 2$ . Therefore the function

$$Y(\theta) = \exp(-\varepsilon(\theta)) \quad (2.7)$$

is analytic and non-zero in this strip and at  $\text{Re } \theta \rightarrow \infty$  behaves as

$$Y(\theta) \sim \exp(-m R e^\theta / 2) \quad (2.8)$$

The asymptotic at  $\text{Re } \theta \rightarrow -\infty$  is related to (2.8) by the symmetry  $Y(\theta) = Y(-\theta)$ . Let us define another even function

$$X(\theta) = \exp \left[ -\frac{mR}{2 \sin \pi p} \cosh \theta + \int \frac{\log(1 + Y(\theta'))}{\cosh(\theta - \theta')} \frac{d\theta'}{2\pi} \right] \quad (2.9)$$

which is obviously analytic and non-zero in the strip  $|\text{Im } \theta| < \pi/2$  and at  $\text{Re } \theta \rightarrow \infty$  in this strip

$$X(\theta) \sim \exp \left( -\frac{mR}{4 \sin \pi p} \exp \theta \right) \quad (2.10)$$

From the TBA equation it follows that

$$X(\theta + i\pi/2) X(\theta - i\pi/2) = Y(\theta) \quad (2.11)$$

**2.** In fact on the real axis  $Y(\theta)$  is real and positive and therefore we expect a strip  $|\text{Im } \theta| < \epsilon$  with some finite  $\epsilon > 0$  where  $1 + Y(\theta) \neq 0$ . Therefore the analyticity condition for  $X(\theta)$  can be extended to the strip  $|\text{Im } \theta| < \pi/2 + \epsilon$ . This is enough to prove the relation

$$X(\theta + i\pi/2) X(\theta - i\pi/2) = 1 + Y(\theta) \quad (2.12)$$

The functional equation

$$X(\theta + i\pi/2) X(\theta - i\pi/2) = 1 + X(\theta + i\pi/2) X(\theta - i\pi/2) \quad (2.13)$$

follows. This relation allows to extend the original analyticity strip  $|\text{Im } \theta| < \pi/2 + \epsilon$  to the strip  $|\text{Im } \theta| < 3\pi/2$  and, as we'll see before long, to the whole complex plane of  $\theta$  so that  $X(\theta)$  is an entire function of  $\theta$ . Notice that from (2.13) it follows that the asymptotic (2.10) holds in the larger strip  $|\text{Im } \theta| < \pi$ . The asymptotic outside this strip is more complicated.

**3.** As a consequence,  $Y(\theta)$  is also entire function of  $\theta$  and satisfies the following functional relation

$$Y(\theta + i\pi/2)Y(\theta - i\pi/2) = (1 + Y(\theta + ia\pi/2))(1 + Y(\theta - ia\pi/2)) \quad (2.14)$$

The last equation is very similar to the functional relations appearing in the TBA study of the integrable perturbed rational conformal field theories (the so called  $Y$ -systems). Typically such  $Y$ -systems imply a periodicity of the  $Y$ -functions in  $\theta$  with some imaginary period related to the scale dimension  $\Delta$  of the perturbing operator (see e.g., [8, 9]). This periodicity in order entails special “perturbative” structure of the short distance  $R \rightarrow 0$  behavior of the ground state energy  $E(R)$ . Namely, up to one exceptional term, it is a regular expansion in powers of  $R^{2-2\Delta}$

$$E(R) = -\mathcal{E}_{\text{vac}}R - \frac{\pi}{6R} \sum_{n=0}^{\infty} c_n R^{(2-2\Delta)n}; \quad R \rightarrow 0 \quad (2.15)$$

where  $\mathcal{E}_{\text{vac}}$  is the infinite volume vacuum energy of the model. Unlike this typical situation, the  $Y$ -system (2.14) or the  $X$ -system (2.13) does not imply any apparent periodic structure of  $Y(\theta)$  in  $\theta$ . As a manifestation of this peculiarity, the  $R \rightarrow 0$  behavior of  $E(R)$  is different from (2.15) and includes softer logarithmic corrections [10]

$$E(R) = -\mathcal{E}R - \frac{\pi}{6R} \left( 1 - \frac{3\pi^2 p(1-p)}{2 \log^2 R} + O(\log^{-3} R) \right); \quad R \rightarrow 0 \quad (2.16)$$

The purpose of the next two sections is to reveal two hidden periodic structures (with different periods) of the  $Y$ -system (2.14).

### 3. Discrete Liouville equation

In this section I discuss the following two-dimensional non-linear finite-difference equation for the function  $X(u, v)$

$$X(u+1, v)X(u-1, v) = 1 + X(u, v+1)X(u, v-1) \quad (3.1)$$

which is apparently resemblent of the functional  $X$ -system (2.13). In the next section we'll see how some of the results for (3.1) can be specialized to our TBA problem. Equation (3.1) is a particular case of Hirota difference equation [11]. The constructions of this section can be found in [12] (see also [13]) where more general difference system is analysed. They appeared also in a quite close context in [14].

Equation (3.1) can be considered as a discretisation of the hyperbolic Liouville equation

$$\partial_u^2 \varphi - \partial_v^2 \varphi = -e^{2\varphi} \quad (3.2)$$

Indeed, let  $X(u, v) = \exp(-\varphi(u, v))$  and let  $\varphi(u, v)$  be large and negative. Then eq.(3.1) is approximated by

$$\varphi(u+1, v) + \varphi(u-1, v) - \varphi(u, v+1) - \varphi(u, v-1) = -\exp(\varphi(u, v+1) + \varphi(u, v-1)) \quad (3.3)$$

In the long-wave limit this is reduced to (3.2). As we'll see below, eq.(3.1) is in many respects very similar to the Liouville equation. It seems quite natural to call it the discrete Liouville equation [15].

Let me remind well known construction of a local solution to eq.(3.2).

**1a.** It is convenient to use the light cone variables  $x^+ = u + v$  and  $x^- = u - v$ , so that  $\partial_+ = (\partial_u + \partial_v)/2$ ;  $\partial_- = (\partial_u - \partial_v)/2$  and (3.2) reads

$$4\partial_+\partial_-\varphi = -e^{2\varphi} \quad (3.4)$$

Let  $\varphi$  be a local solution of (3.4). Define

$$\begin{aligned} t &= -(\partial_+\varphi)^2 + \partial_+^2\varphi \\ \tilde{t} &= -(\partial_-\varphi)^2 - \partial_-^2\varphi \end{aligned} \quad (3.5)$$

As a consequence of eq.(3.4) we have

$$\partial_- t = \partial_+ \tilde{t} = 0 \quad (3.6)$$

so that  $t(x^+)$  and  $\tilde{t}(x^-)$  are respectively functions of only  $x^+$  and  $x^-$ .

**2a.** Field  $X = \exp(-\varphi)$  satisfies two linear differential equations

$$(\partial_+^2 + t(x^+))X(u, v) = 0; \quad (\partial_-^2 + \tilde{t}(x^-))X(u, v) = 0 \quad (3.7)$$

**3a.** Let  $Q_\pm(x)$  and  $\tilde{Q}_\pm(x)$  be linearly independent solutions to the ordinary differential equations

$$\begin{aligned} (\partial_x^2 + t(x))Q_\pm(x) &= 0 \\ (\partial_x^2 + \tilde{t}(x))\tilde{Q}_\pm(x) &= 0 \end{aligned} \quad (3.8)$$

normalized in the way that

$$\begin{aligned} \partial_x Q_+(x)Q_-(x) - Q_+(x)\partial_x Q_-(x) &= 1/2 \\ \partial_x \tilde{Q}_+(x)\tilde{Q}_-(x) - \tilde{Q}_+(x)\partial_x \tilde{Q}_-(x) &= 1/2 \end{aligned} \quad (3.9)$$

A local solution of (3.4) can be constructed as

$$\exp(-\varphi(u, v)) = Q_+(x^+)\tilde{Q}_+(x^-) + Q_-(x^+)\tilde{Q}_-(x^-) \quad (3.10)$$

**4a.** Introduce the functions

$$F(x) = \frac{Q_+(x)}{Q_-(x)} ; \quad G(x) = -\frac{\tilde{Q}_-(x)}{\tilde{Q}_+(x)} \quad (3.11)$$

The solution (3.10) can be rewritten as

$$\exp 2\varphi(u, v) = \frac{4F'(x^+)G'(x^-)}{(F(x^+) - G(x^-))^2} \quad (3.12)$$

Notice also that in terms of  $F$  and  $G$

$$t(x) = -2\{F(x), x\} ; \quad \tilde{t}(x) = -2\{G(x), x\} \quad (3.13)$$

where

$$\{f(x), x\} = \frac{f'''}{f'} - \frac{3}{2} \left( \frac{f''}{f'} \right)^2 \quad (3.14)$$

is the Schwarz derivative.

Now let us turn to the discrete Liouville equation (3.1). Defining, similarly to eq.(2.11),

$$\begin{aligned} Y(u, v) &= X(u, v+1)X(u, v-1) \\ 1 + Y(u, v) &= X(u+1, v)X(u-1, v) \end{aligned} \quad (3.15)$$

we arrive at the finite difference equation analogous to (2.14)

$$Y(u+1, v)Y(u-1, v) - (1 + Y(u, v+1))(1 + Y(u, v-1)) \quad (3.16)$$

**1b.** Introduce

$$\begin{aligned} T(u, v) &= \frac{X(u+1, v+1) + X(u-1, v-1)}{X(u, v)} \\ \tilde{T}(u, v) &= \frac{X(u+1, v-1) + X(u-1, v+1)}{X(u, v)} \end{aligned} \quad (3.17)$$

As a consequence of eq.(3.1) we obtain

$$\begin{aligned} T(u+1, v-1) &= T(u, v) \\ \tilde{T}(u+1, v+1) &= \tilde{T}(u, v) \end{aligned} \quad (3.18)$$

so that  $T = T(u+v)$  and  $\tilde{T} = \tilde{T}(u-v)$ . In the continuous limit these objects are related to (3.5) as  $T(u) = 2 - 4t(u) + \dots$ ;  $\tilde{T}(u) = 2 - 4\tilde{t}(u) + \dots$  [14].

**2b.** Eqs.(3.17) can be rewritten as (similarly to (3.7))

$$\begin{aligned} X(u+1, v+1) + X(u-1, v-1) &= T(u+v)X(u, v) \\ X(u+1, v-1) + X(u-1, v+1) &= \tilde{T}(u-v)X(u, v) \end{aligned} \quad (3.19)$$

**3b.** Let  $Q_{\pm}(u)$  and  $\tilde{Q}_{\pm}(u)$  be linearly independent solutions of the second order finite difference equations

$$\begin{aligned} Q_{\pm}(u+2) + Q_{\pm}(u-2) &= T(u)Q_{\pm}(u) \\ \tilde{Q}_{\pm}(u+2) + \tilde{Q}_{\pm}(u-2) &= \tilde{T}(u)\tilde{Q}_{\pm}(u) \end{aligned} \quad (3.20)$$

normalized by the “quantum Wronskians”

$$\begin{aligned} Q_+(u+1)Q_-(u-1) - Q_+(u-1)Q_-(u+1) &= 1 \\ \tilde{Q}_+(u+1)\tilde{Q}_-(u-1) - \tilde{Q}_+(u-1)\tilde{Q}_-(u+1) &= 1 \end{aligned} \quad (3.21)$$

Then it is verified that

$$X(u, v) = Q_+(u+v)\tilde{Q}_+(u-v) + Q_-(u+v)\tilde{Q}_-(u-v) \quad (3.22)$$

is a local solution of the discrete Liouville equation (3.1).

**4b.** Introduce the functions

$$F(u) = \frac{Q_+(u)}{Q_-(u)}; \quad G(u) = -\frac{\tilde{Q}_-(u)}{\tilde{Q}_+(u)} \quad (3.23)$$

which can be used to present the local solution (3.22) in the form

$$\begin{aligned} Y(u, v) &= \frac{(F(u+v+1) - G(u-v-1))(F(u+v-1) - G(u-v+1))}{(F(u+v+1) - F(u+v-1))(G(u-v+1) - G(u-v-1))} \\ 1 + Y(u, v) &= \frac{(F(u+v+1) - G(u-v+1))(F(u+v-1) - G(u-v-1))}{(F(u+v+1) - F(u+v-1))(G(u-v+1) - G(u-v-1))} \end{aligned} \quad (3.24)$$

Let me mention also the discrete analogue of the Schwarzian derivative (3.13)

$$T(u+1)T(u-1) = \frac{(F(u+3) - F(u-1))(F(u+1) - F(u-3))}{(F(u+3) - F(u+1))(F(u-1) - F(u-3))} \quad (3.25)$$

## 4. Application to TBA

The above constructions for the discrete Liouville equation can be translated for the ShG  $X$ -system (2.13) we are interested in. Let us require the following periodicity condition for  $X(u, v)$  in (3.1)

$$X(u+a, v+1) = X(u, v) \quad (4.1)$$

with some parameter  $a$  (at this point we start to diverge from the lines of [14]). With this periodicity eq.(3.1) reads

$$X(u+1, v)X(u-1, v) = 1 + X(u+a, v)X(u-a, v) \quad (4.2)$$

Here  $v$  can be considered as a parameter. Suppressing this redundant dependence and rescaling  $u$  as

$$\theta = i\pi u/2 \quad (4.3)$$

we are back to the ShG  $X$  system in the form (2.13).

From  $X(\theta)$  the two functions  $T(\theta)$  and  $\tilde{T}(\theta)$  are readily restored as

$$\begin{aligned} T(\theta) &= \frac{X(\theta + i\pi(1-a)/2) + X(\theta - i\pi(1-a)/2)}{X(\theta)} \\ \tilde{T}(\theta) &= \frac{X(\theta + i\pi(1+a)/2) + X(\theta - i\pi(1+a)/2)}{X(\theta)} \end{aligned} \quad (4.4)$$

The “holomorphic” property (3.18) is translated to the following periodicity of these functions

$$\begin{aligned} T(\theta + i\pi(1+a)/2) &= T(\theta) \\ \tilde{T}(\theta + i\pi(1-a)/2) &= \tilde{T}(\theta) \end{aligned} \quad (4.5)$$

Notice that the period  $i\pi/(1+b^2)$  of  $T$  corresponds to the negative dimension  $\Delta = -b^2$  of the perturbing operator in (1.1). As it can be anticipated from the self-duality of ShG, the second period  $i\pi b^2/(1+b^2)$  of  $\tilde{T}$  is related to the dimension  $\tilde{\Delta} = -b^{-2}$  of the “dual” exponentials  $\exp(\pm 2\phi/b)$ .

As it is discussed in sect.2  $X(\theta)$  is analytic and non-zero in the strip  $|\text{Im } \theta| < \pi/2$  and analytic in the larger strip  $|\text{Im } \theta| < 3\pi/2$ . Therefore  $T(\theta)$  and  $\tilde{T}(\theta)$  are analytic in the strip  $|\text{Im } \theta| < \pi/2$  and by periodicity (4.5) are entire functions of  $\theta$ . It follows from (4.4) that  $X(\theta)$  is an entire function of  $\theta$  too.

The asymptotics at  $\text{Re } \theta \rightarrow \infty$  follow from (2.10) and (4.4)

$$\begin{aligned} T(\theta) &\sim \exp\left(\frac{mR \exp(\theta - i\pi(1-p)/2)}{4 \cos(\pi p/2)}\right) \quad \text{in the strip } 0 < \text{Im } \theta < \pi(1+a)/2 \\ \tilde{T}(\theta) &\sim \exp\left(\frac{mR \exp(\theta - i\pi p/2)}{4 \sin(\pi p/2)}\right) \quad \text{in the strip } 0 < \text{Im } \theta < \pi(1-a)/2 \end{aligned} \quad (4.6)$$

The real axis  $\text{Im } \theta = 0$  is a Stokes line and here

$$\begin{aligned} T(\theta) &\sim 2 \exp\left(\frac{mR}{4} \tan(\pi p/2) e^\theta\right) \cos\left(\frac{mR}{4} \exp \theta\right) \\ \tilde{T}(\theta) &\sim 2 \exp\left(\frac{mR}{4} \cot(\pi p/2) e^\theta\right) \cos\left(\frac{mR}{4} \exp \theta\right) \end{aligned} \quad (4.7)$$

The  $\text{Re } \theta \rightarrow \infty$  asymptotic in the whole plane of  $\theta$  is restored from the periodicity (4.5). Following (4.7) both  $T$  and  $\tilde{T}$  have infinite number of zeroes on the real axis located at  $\theta = \pm\theta_n$ ,  $n = 1, 2, \dots, \infty$  with  $\theta_n \sim \log(2\pi n/mR) + O(1/n)$  at  $n \rightarrow \infty$ . The half-period

shifted functions  $T(\theta + i\pi(1-p)/2)$  and  $\tilde{T}(\theta + i\pi p/2)$  are also real at real  $\theta$  and at  $\theta \rightarrow \infty$  behave as

$$\begin{aligned} T(\theta + i\pi(1-p)/2) &\sim \exp\left(\frac{mR}{4\cos(\pi p/2)}e^\theta\right) \\ \tilde{T}(\theta + i\pi p/2) &\sim \exp\left(\frac{mR}{4\sin(\pi p/2)}e^\theta\right) \end{aligned} \quad (4.8)$$

Analytic properties of  $T$  and  $\tilde{T}$  allow the following convergent expansions

$$\begin{aligned} T(\theta) &= \sum_{-\infty}^{\infty} T_n \exp(2nQb\theta) \\ \tilde{T}(\theta) &= \sum_{-\infty}^{\infty} \tilde{T}_n \exp(2nQ\theta/b) \end{aligned} \quad (4.9)$$

with real  $T_n$  and  $\tilde{T}_n$ . From the symmetry of the original TBA equations  $T$  and  $\tilde{T}$  both even functions of  $\theta$  so that in our present case  $T_n = T_{-n}$  and  $\tilde{T}_n = \tilde{T}_{-n}$ . One can read-off the leading large  $n$  behavior of the coefficients  $T_n$  and  $\tilde{T}_n$  from the asymptotics (4.6)

$$\begin{aligned} T_n &\sim (-)^n \sqrt{\frac{bQ}{\pi}} n^{-2Qbn-1/2} \left( e \frac{mR}{8\pi bQ \cos(\pi p/2)} \right)^{2Qbn} \\ \tilde{T}_n &\sim (-)^n \sqrt{\frac{Q}{\pi b}} n^{-2Qn/b-1/2} \left( e \frac{bmR}{8\pi Q \sin(\pi p/2)} \right)^{2Qn/b} \end{aligned} \quad (4.10)$$

So far the constructions were explicitly based on the integral equation (2.3). The rest of the section is more speculative. Suppose that for  $T(\theta)$  and  $\tilde{T}(\theta)$  constructed as in (4.4) we can find  $Q_{\pm}(\theta)$  and  $\tilde{Q}_{\pm}(\theta)$  which solve

$$\begin{aligned} Q_{\pm}(\theta + i\pi) + Q_{\pm}(\theta - i\pi) &= T(\theta)Q_{\pm}(\theta) \\ \tilde{Q}_{\pm}(\theta + i\pi) + \tilde{Q}_{\pm}(\theta - i\pi) &= T(\theta)\tilde{Q}_{\pm}(\theta) \end{aligned} \quad (4.11)$$

and are the ‘‘Bloch waves’’ with respect to the periods of  $T$  and  $\tilde{T}$  respectively

$$\begin{aligned} Q_{\pm}(\theta + i\pi(1+a)/2) &= \exp(\pm 2i\pi P/Q) Q_{\pm}(\theta) \\ \tilde{Q}_{\pm}(\theta + i\pi(1-a)/2) &= \exp(\pm 2i\pi P/Q) \tilde{Q}_{\pm}(\theta) \end{aligned} \quad (4.12)$$

with some Floquet index  $P$ . Let them be normalized by the quantum Wronskians

$$\begin{aligned} Q_+(\theta + i\pi/2)Q_-(\theta - i\pi/2) - Q_+(\theta - i\pi/2)Q_-(\theta + i\pi/2) &= 1 \\ \tilde{Q}_+(\theta + i\pi/2)\tilde{Q}_-(\theta - i\pi/2) - \tilde{Q}_+(\theta - i\pi/2)\tilde{Q}_-(\theta + i\pi/2) &= 1 \end{aligned} \quad (4.13)$$

Then formally

$$X(\theta) = Q_+(\theta)\tilde{Q}_+(\theta) + Q_-(\theta)\tilde{Q}_-(\theta) \quad (4.14)$$

solves eqs.(4.4) as well as the  $X$ -system (2.13).

Unfortunately at present I know no effective means to construct these  $Q$ -functions. Moreover, there are serious doubts that the objects satisfying both (4.11) and (4.12) can be constructed in any sense, at least at rational values of  $b^2$ . I hope to say something more definite on this point in close future.

## 5. Large $\text{Re } \theta$ asymptotics

Let me comment a little more about the  $\text{Re } \theta \rightarrow \infty$  asymptotics (with  $\text{Im } \theta$  fixed) of the function  $X(\theta)$  in the whole complex plane. In principle it can be restored from the asymptotic (2.10) in the strip  $|\text{Im } \theta| \leq \pi/2$  using the functional relation (2.13) or, more conveniently, the relations (4.4) together with the asymptotics (4.6). The asymptotics is always of the form

$$X(\theta) \sim \exp(A(\text{Im } \theta) \exp(\text{Re } \theta)) \quad (5.1)$$

with some complex function  $A(\eta)$  of real variable  $\eta = \text{Im } \theta$ . Apparently  $\text{Re } A(\eta)$  controls the rate of growth of the absolute value of  $X$ . At  $|\eta| < \pi/2$  we have

$$A(\eta) = -\frac{mR}{4 \sin \pi p} e^{i\eta} \quad (5.2)$$

It follows from (4.4) that  $A(\eta)$  satisfies two functional relations

$$A(\eta + \pi(1-a)/2) = \begin{cases} A(\eta) + \sigma(\eta) & \text{if } \text{Re}(A(\eta) + \sigma(\eta)) > \text{Re } A(\eta + \pi(1-a)/2) \\ A(\eta + \pi(1-a)/2) & \text{otherwise} \end{cases} \quad (5.3)$$

$$A(\eta + \pi(1+a)/2) = \begin{cases} A(\eta) + \tilde{\sigma}(\eta) & \text{if } \text{Re}(A(\eta) + \tilde{\sigma}(\eta)) > \text{Re } A(\eta + \pi(1+a)/2) \\ A(\eta + \pi(1+a)/2) & \text{otherwise} \end{cases}$$

where the functions  $\sigma(\eta)$  and  $\tilde{\sigma}(\eta)$  control the asymptotics of  $T(\theta)$  and  $\tilde{T}(\theta)$ . They are defined as

$$\sigma(\eta) = \frac{mR}{4 \cos(\pi p/2)} \exp(i\eta - i\pi(1-p)/2) \quad \text{at } 0 \leq \eta < (1+a)/2 \quad (5.4)$$

$$\tilde{\sigma}(\eta) = \frac{mR}{4 \sin(\pi p/2)} \exp(i\eta - i\pi p/2) \quad \text{at } 0 \leq \eta < (1-a)/2$$

and continued outside these regions periodically as  $\tilde{\sigma}(\eta + \pi(1-a)/2) = \tilde{\sigma}(\eta)$  and  $\sigma(\eta + \pi(1+a)/2) = \sigma(\eta)$ . Both  $\sigma(\eta)$  and  $\tilde{\sigma}(\eta)$  jump by  $-imR/2$  at  $\eta = \pi(1+a)n/2$ ,  $n \in \mathbb{Z}$  and  $\eta = \pi(1-a)n/2$ ,  $n \in \mathbb{Z}$  respectively. This corresponds to the limiting density of zeroes prescribed by (4.7).

A common solution to (5.3) exists. Generally the solution is discontinuous at all values  $\eta = \pm\pi(m(1+a)/2 + n(1-a)/2)$  with arbitrary positive integers  $n$  and  $m$ . At each

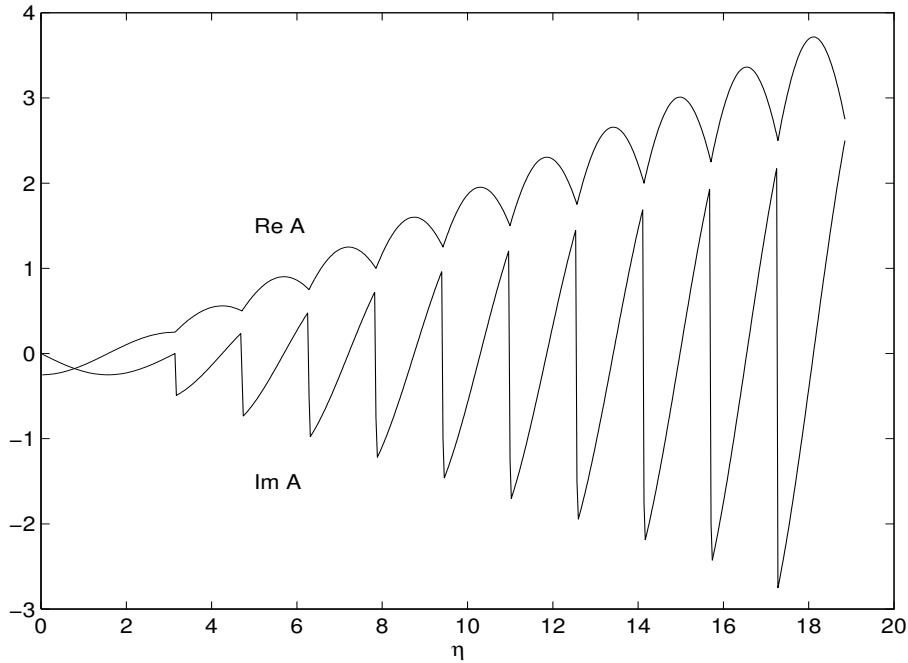


Figure 1: Real and imaginary parts of  $A(\eta)/mR$  at  $b^2 = 1$ .

such point the imaginary part  $\text{Im } A$  jumps down by  $-mR/2$  indicating an asymptotic line of accumulation of zeroes of  $X(\theta)$ , the asymptotic density being the same as that of the functions  $T$  and  $\tilde{T}$  (4.7). The real part of  $A$  at these points is continuous itself but has discontinuities in the first derivative. The first Stokes line appears at  $\eta = \pi$ .

At large  $\eta$  the structure is qualitatively different dependent on the arithmetic nature of parameter  $b^2$ . If it is a rational number the periods of  $T$  and  $\tilde{T}$  are commensurable. Some of the discontinuities merge forming multiple jumps in the imaginary part. The solution  $A(\theta)$  bears a regular “quasiperiodic” structure with the common period of  $T$  and  $\tilde{T}$ . For irrational  $b^2$  the periods are incommensurable and as  $\eta \rightarrow \infty$  the singularities are more and more dense, the solution having quite irregular behavior.

In fig.1 real and imaginary parts of  $A(\eta)$  are plotted for the simplest (self-dual) case  $b = 1$ . Both periods are equal to  $\pi/2$ . The discontinuities are located at  $\eta = \pm\pi(n + 1)/2$ ,  $n = 1, 2, \dots$  where the imaginary part jumps by  $-mRn/2$ . Contrary to the location of zeroes of  $T$ , zeroes of  $X$  cannot lie exactly on the lines  $\text{Im } \theta = \text{const}$ , at least for the first line  $\eta = \pi$ . Indeed, in the case  $b^2 = 1$  it follows from the functional relation that at real  $\theta$

$$|X(\theta + i\pi)|^2 = X^2(\theta) + T^2(\theta) \quad (5.5)$$

which is strictly positive.

Another rational situation  $b^2 = 1/2$  corresponds to the periods  $\pi/3$  and  $2\pi/3$ . Function  $A(\eta)$  is plotted in fig.2. The structure is again quite regular, the discontinuities occurring at

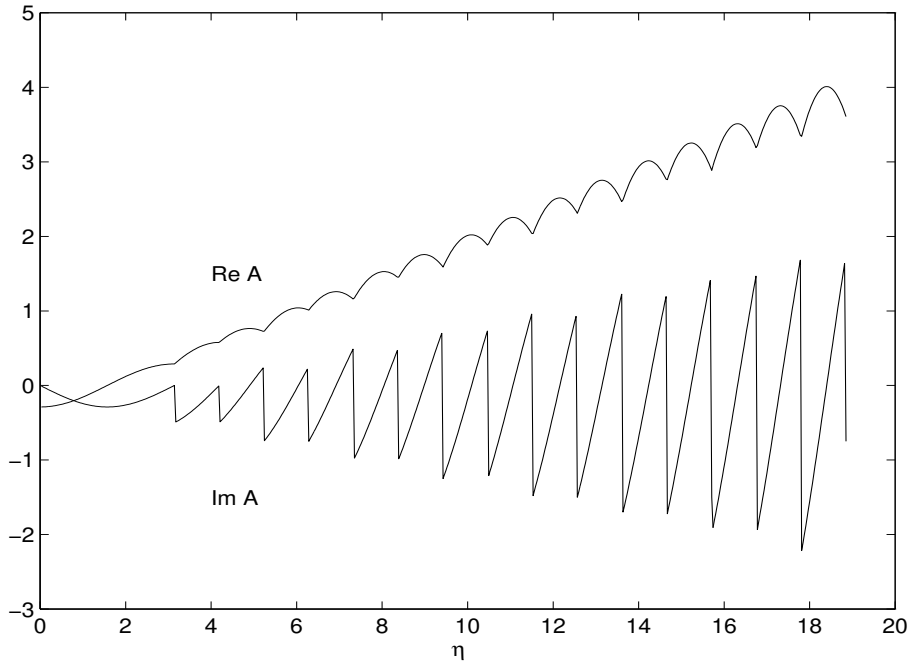


Figure 2: Real and imaginary parts of  $A(\eta)/mR$  at  $b^2 = 1/2$ .

$\eta = \pi + n\pi/3$ ,  $n = 1, 2, \dots$ , the first two discontinuities in  $\text{Im } A$  being  $-mR/2$ , next two are twice of this amount, then next two trice, etc.

With irrational  $b^2$  the picture is far less regular. To illustrate what happens when  $b^2$  slightly deviates from a simple rational number, in fig.3 we plot  $A(\eta)$  for  $b^2 = 0.8086\dots$  which is reasonably close to 1. Comparing with fig.1 we see that the first discontinuity at  $\eta = \pi$  remains basically the same while the second (double) discontinuity at  $\eta = 3\pi/2$  splits in two simple ones, the third (triple) splits in three simple jumps etc. At some point these splitted groups come to overlap and the picture turns irregular.

## 6. Staircase situation

The staircase model [10] is a formal analytic continuation of ShG to complex values of the parameter  $b$  such that  $b^{-1} = b^*$ . Although the physical content of this continuation is not completely clear from the field theory point of view, the TBA equation (2.3) remains completely sensible and this continuation of (2.3) can be studied on its own footing. The effective central charge (2.2) is still real and develops sometimes quite intriguing patterns (see [10]).

In [10] the complex  $b$  has been parameterised as follows

$$b^2 = \frac{1 + 2i\theta_0/\pi}{1 - 2i\theta_0/\pi} \quad (6.1)$$

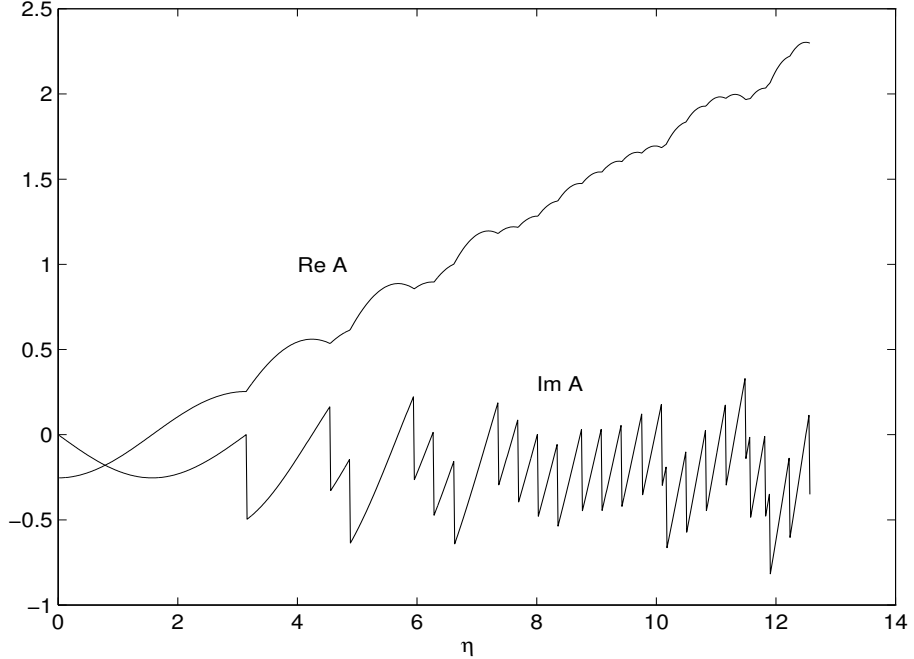


Figure 3: Real and imaginary parts of  $A(\eta)/mR$  at  $b^2 = 0.8086 \dots$

with real  $0 \leq \theta_0 < \infty$ . Parameter  $p$  of (1.3) now reads

$$p = \frac{1}{2} + \frac{i\theta_0}{\pi} \quad (6.2)$$

while  $1 - p = p^*$  and  $a$  defined in (2.6) is purely imaginary  $a = -2i\theta_0/\pi$ . The TBA kernel (2.4) is real and reads

$$\varphi(\theta) = \frac{1}{2\pi} \left( \frac{1}{\cosh(\theta + \theta_0)} + \frac{1}{\cosh(\theta - \theta_0)} \right) \quad (6.3)$$

with the Fourier transform

$$\varphi(\omega) = \frac{\cos(\omega\theta_0)}{\cosh(\pi\omega/2)} \quad (6.4)$$

After these substitution the integral equation (2.3) determines real-analytic functions  $\varepsilon(\theta)$ ,  $Y(\theta)$  and, through (2.9), a real-analytic and symmetric  $X(\theta)$  with the asymptotic behavior at  $\text{Re } \theta \rightarrow \infty$  in the strip  $-\pi/2 < \text{Im } \theta < \pi/2$

$$X(\theta) \sim \exp \left( -\frac{mR}{4 \cosh \theta_0} \exp \theta \right) \quad (6.5)$$

The functional equation (2.13) reads now

$$X(\theta + i\pi/2) X(\theta - i\pi/2) = 1 + X(\theta + \theta_0) X(\theta - \theta_0) \quad (6.6)$$

All the considerations of sect.4 can be repeated literally. Function  $X(\theta)$  is still entire as well as  $T(\theta)$  and  $\tilde{T}(\theta)$  defined in eq.(4.4) and the asymptotic (6.5) can be extended to the strip  $-\pi < \text{Im } \theta < \pi$ . The difference is that the periods of  $T(\theta)$  and  $\tilde{T}(\theta)$

$$\begin{aligned} T(\theta + \tau) &= T(\theta) ; \quad \tau = i\pi(1+a)/2 = i\pi/2 + \theta_0 \\ \tilde{T}(\theta + \tilde{\tau}) &= \tilde{T}(\theta) ; \quad \tilde{\tau} = i\pi(1-a)/2 = i\pi/2 - \theta_0 \end{aligned} \quad (6.7)$$

are now complex  $\tau = -\tilde{\tau}^*$ . Functions  $T(\theta) = T(-\theta)$  and  $\tilde{T}(\theta) = \tilde{T}(-\theta)$  are still symmetric but no more real analytic. Instead

$$T^*(\theta) = \tilde{T}(\theta^*) \quad (6.8)$$

Expansions similar to (4.9)

$$\begin{aligned} T(\theta) &= \sum_{-\infty}^{\infty} T_n \exp(2i\pi n\theta/\tau) \\ \tilde{T}(\theta) &= \sum_{-\infty}^{\infty} \tilde{T}_n \exp(2i\pi n\theta/\tilde{\tau}) \end{aligned} \quad (6.9)$$

are convergent and  $T_n = T_{-n}$ ;  $\tilde{T}_n = \tilde{T}_{-n}$ . Instead of being real as in the real  $b$  case, these coefficients are complex conjugate  $T_n^* = \tilde{T}_n$ .

In the strip  $0 < \text{Im } \theta < \pi/2$  the following  $\text{Re } \theta \rightarrow \infty$  asymptotics holds for  $T$  and  $\tilde{T}$

$$\begin{aligned} T(\theta) &\sim X(\theta + \tilde{\tau})/X(\theta) \sim \exp\left(\frac{mR(1 - i \exp(-\theta_0))}{4 \cosh \theta_0} e^\theta\right) \\ \tilde{T}(\theta) &\sim X(\theta + \tau)/X(\theta) \sim \exp\left(\frac{mR(1 - i \exp(\theta_0))}{4 \cosh \theta_0} e^\theta\right) \end{aligned} \quad (6.10)$$

The asymptotic changes at the Stokes line along the real axis where

$$\begin{aligned} T(\theta) &\sim 2 \exp\left(\frac{mR(1 + i \sinh \theta_0)}{4 \cosh \theta_0} e^\theta\right) \cos\left(\frac{mR}{4} e^\theta\right) \\ \tilde{T}(\theta) &\sim 2 \exp\left(\frac{mR(1 - i \sinh \theta_0)}{4 \cosh \theta_0} e^\theta\right) \cos\left(\frac{mR}{4} e^\theta\right) \end{aligned} \quad (6.11)$$

and we observe again an infinite sequence of zeroes accumulating at infinity, the density being the same as in the real  $b$  case of sect.5. In the strips  $\pi n/2 < \text{Im } \theta < \pi(n+1)/2$  (with arbitrary

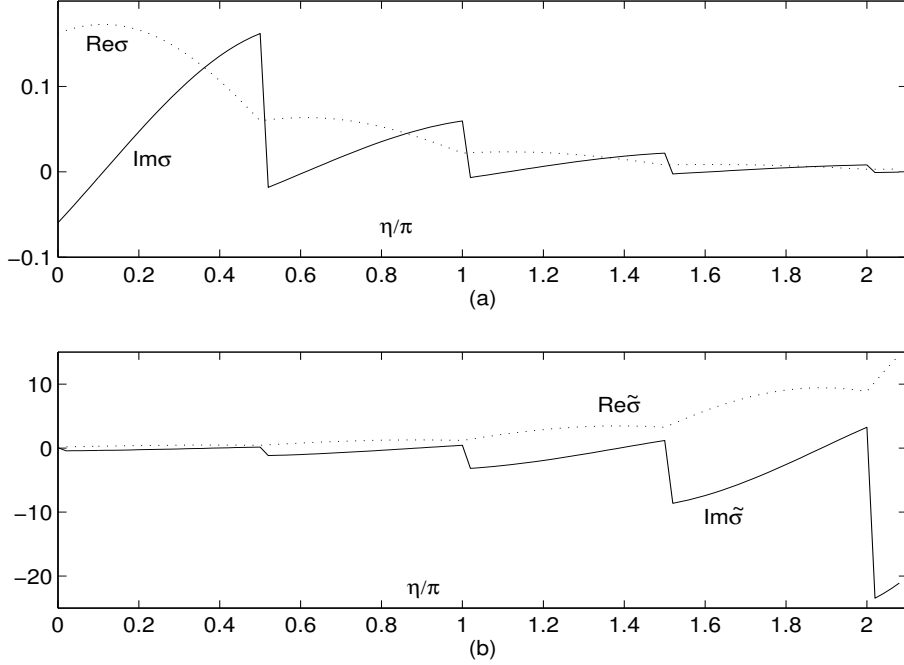


Figure 4: Real and imaginary parts of  $\sigma(\eta)/mR$  (a) and  $\tilde{\sigma}(\eta)/mR$  (b). The staircase example for  $\theta_0 = 1$ .

integer  $n$ ) the  $\text{Re}\theta \rightarrow \infty$  asymptotics follow from the periodicity (6.7). In particular, along the lines  $\text{Im}\theta = in\pi/2$  (with any integer  $n$ ) we'll have

$$\begin{aligned} T(\theta) &\sim 2 \exp \left( \frac{mR(1 + i \sinh \theta_0)}{4 \cosh \theta_0} e^{\text{Re}\theta - n\theta_0} \right) \cos \left( \frac{mR}{4} e^{\text{Re}\theta - n\theta_0} \right) \\ \tilde{T}(\theta) &\sim 2 \exp \left( \frac{mR(1 - i \sinh \theta_0)}{4 \cosh \theta_0} e^{\text{Re}\theta + n\theta_0} \right) \cos \left( \frac{mR}{4} e^{\text{Re}\theta + n\theta_0} \right) \end{aligned} \quad (6.12)$$

Functions  $\sigma(\eta)$  and  $\tilde{\sigma}(\eta)$  which control the asymptotics of  $T$  and  $\tilde{T}$  at  $\text{Re}\theta \rightarrow \infty$

$$\begin{aligned} T(\theta) &\sim \exp(\sigma(\text{Im}\theta) e^{\text{Re}\theta}) \\ \tilde{T}(\theta) &\sim \exp(\tilde{\sigma}(\text{Im}\theta) e^{\text{Re}\theta}) \end{aligned} \quad (6.13)$$

are plotted in fig.4 for the case  $\theta_0 = 1$ . It's enough to present them for  $\eta \geq 0$  since  $\sigma(-\eta) = \tilde{\sigma}^*(\eta)$ . The imaginary part of  $\sigma(\eta)$  jumps at the points  $\eta = n\pi/2$  by the amount  $-mR \exp(-n\theta_0)/2$ , in accord with the density of zeroes predicted by (6.12). Unlike the previously considered case of real  $b$ , in the staircase situation the zeroes of  $T$  and  $\tilde{T}$  are not located exactly at the lines  $\text{Im}\theta = in\pi/2$  but slightly shifted in the imaginary direction (we'll observe this deviation numerically in the next section) and approach these lines asymptotically as  $\text{Re}\theta \rightarrow \infty$ .

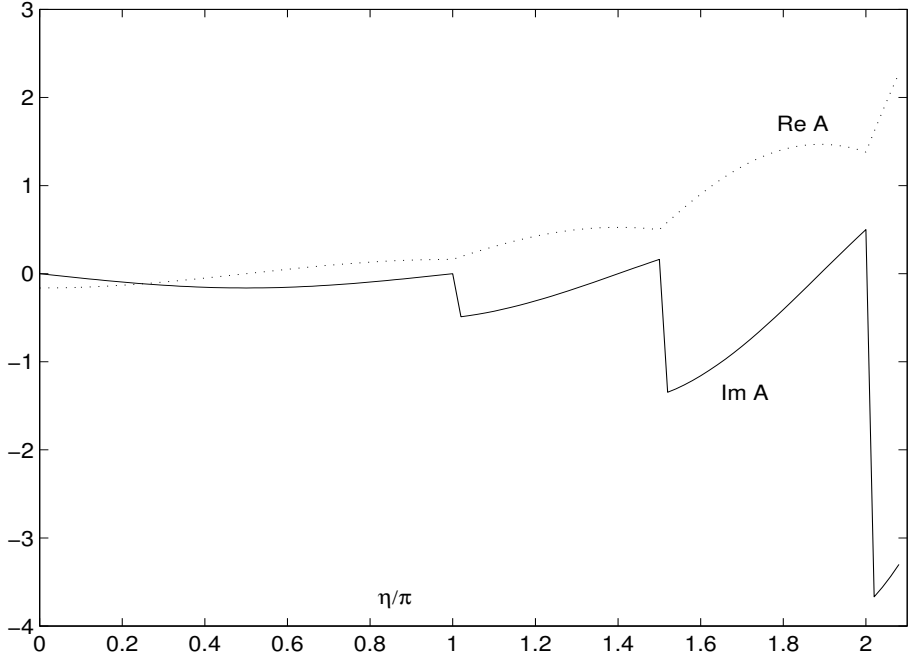


Figure 5: A staircase example of  $A(\eta)/mR$  at  $\theta_0 = 1$ .

Notice also that e.g.  $T(\theta)$  is a single valued function of  $\xi = \exp(2i\pi\theta/\tau)$ . In the complex plane of this variable the asymptotic lines of accumulation of zeroes  $\text{Im } \theta = 0$ ;  $\text{Re } \theta \rightarrow \pm\infty$  are parts of the spiral  $|\xi| = \exp(\pi \arg \xi/2\theta_0)$  near which zeroes become dense at  $|\xi| \rightarrow \infty$  or  $|\xi| \rightarrow 0$ , the density growing as  $|\xi|^{\pm(1/4+\theta_0^2/\pi^2)}$  respectively. Therefore the large (or small)  $|\xi|$  asymptotics of  $T(\xi)$  at fixed  $\arg \xi$  is rather complicated.

Large  $\text{Re } \theta$  asymptotic of  $X(\theta)$  at fixed  $\eta = \text{Im } \theta$  is controlled by the function  $A(\eta)$  (see eq.(5.1)). An example corresponding to the case  $\theta_0 = 1$  is presented in fig.5. At the points  $\eta = \pm\pi(n + 1)/2$ ,  $n = 1, 2, \dots$  imaginary part of  $A(\eta)$  has discontinuities equal to  $-mR \sinh(n\theta_0)/(2 \sinh \theta_0)$ . These amounts determine the asymptotic density of zeroes of  $X(\theta)$  along these lines.

## 7. Numerics

Integral equation (2.3) can be easily solved numerically e.g., by iterations. The iterations happen to be well convergent (the convergence is somewhat slower if  $R$  approaches to 0 or the parameter  $p$  is taken very small). In the strip  $|\text{Im } \theta| < \pi/2$  function  $X(\theta)$  can be computed using the integral representation (2.9). This allows to continue  $X(\theta)$  to the whole complex plane iterating the relation (2.13) (in fact at large  $\text{Im } \theta$  it is more convenient to evaluate first  $T(\theta)$  inside its period and then use (4.4)). In the rest of this section we will use the logarithmic scale parameter  $x = \log(mR/2)$  instead of  $R$ .

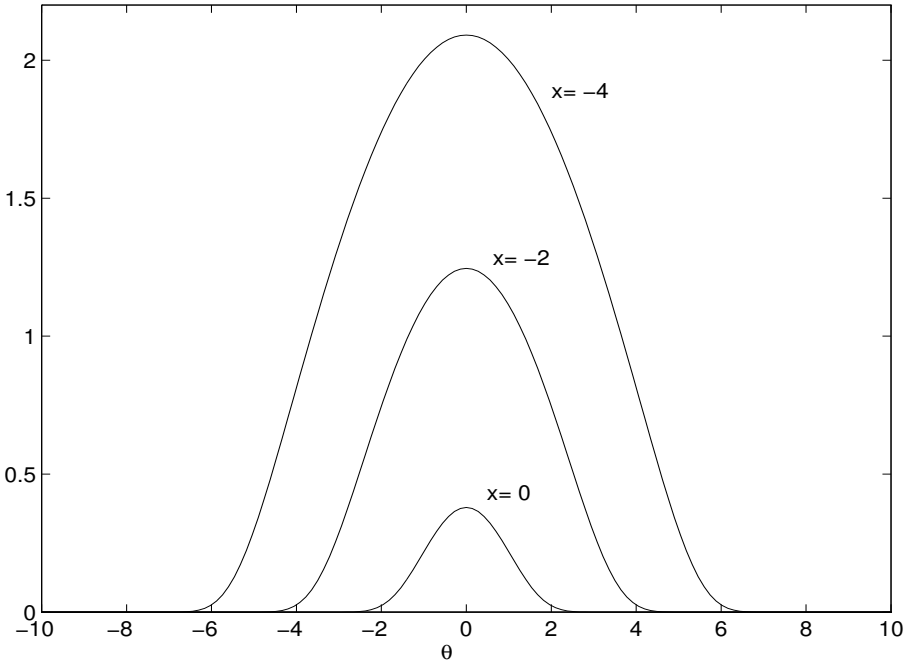


Figure 6: Typical bell-shaped patterns of  $X(\theta)$  on the real axis ( $b^2 = 1$ ).

### 1. Self-dual point $b^2 = 1$ .

In fig.6 several examples of function  $X(\theta)$  on the real axis of  $\theta$  are plotted for different values of  $x$ . Function is typically bell-shaped. As  $x$  becomes large negative the width of the support of the bell as well as its height grow proportionally to  $-x$ . No plateau typical for perturbed rational CFT's is developed.

Few samples of  $T(\theta)$  (which is the same as  $\tilde{T}(\theta)$  at the self-dual point) are presented in fig.7. At  $x$  negative and large enough,  $T$  develops a plateau in the “central region”  $x < \theta < -x$  of the height which approaches slowly to 2 as  $-x$  grows. We'll comment more about this approach below. Outside the central region it starts to oscillate with growing amplitude and frequency. Approach to the asymptotic (4.7) is very fast.

Due to the symmetry  $T(\theta) = T(-\theta)$  this function is real on the imaginary axis too. A couple of examples are plotted in fig.8. At  $x$  essentially negative, when the plateau is well developed in the central region, the mean value  $T_0$  (see eq.(4.9)) is very close to the plateau height, the oscillations around (determined mainly by  $T_1$ ) being very small ( $T_1 \sim R^4$ , see eq.(8.9) below).

Function  $T(\theta)$  is real also at the half-period line  $\text{Im } \theta = \pi/4$ . Again there is a plateau region (at large negative  $x$ ) of the same height as on the real axis. Then  $T(\theta + i\pi/4)$  remains positive and grows following the asymptotic (4.8) (see fig.9). Numerical computations in the whole period strip  $0 \leq \text{Im } \theta < \pi/2$  show no sign of other zeros then those on the real axis.

In fig.10 few examples of  $|X(\theta)|$  in the complex plane at different values of  $\text{Re } \theta$  are plotted vs.  $\text{Im } \theta$  (for  $x = 0$ ). The specific values  $\text{Re } \theta = 1.22$  and  $\text{Re } \theta = 2.25$  are chosen

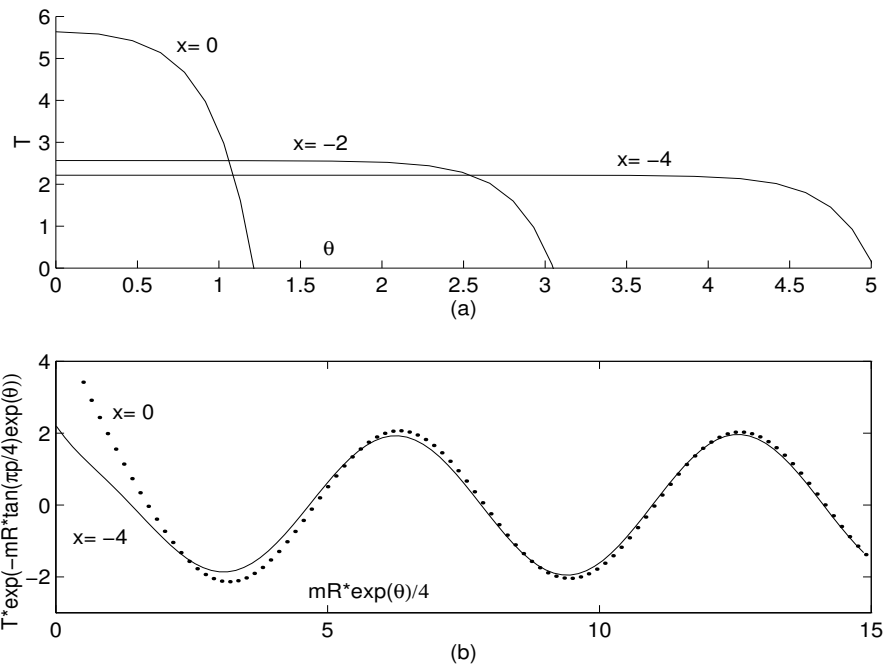


Figure 7: Function  $T(\theta)$  on the real axis ( $b^2 = 1$ ).

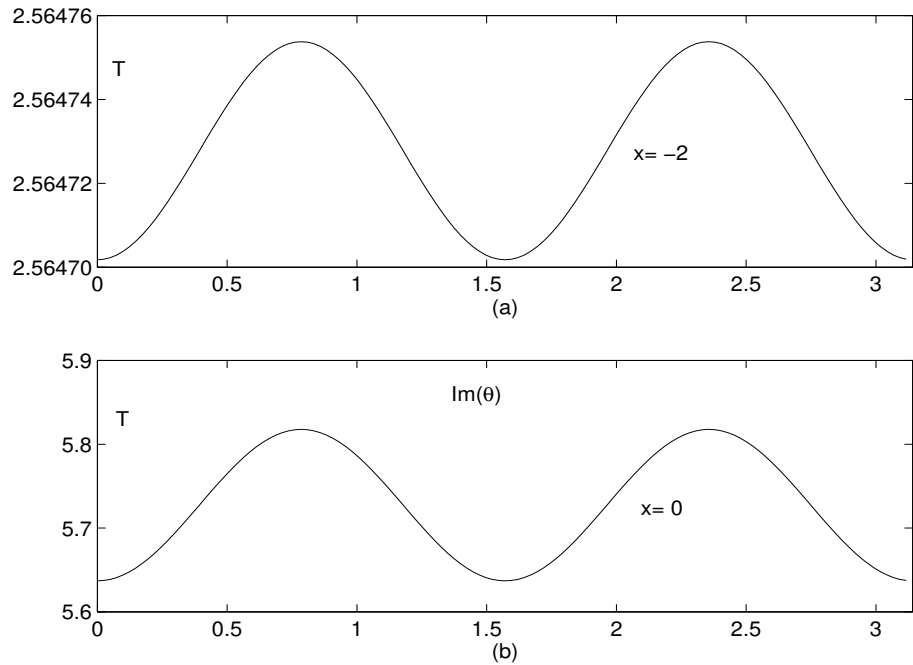


Figure 8: Function  $T(\theta)$  along the imaginary axis ( $b^2 = 1$ ).

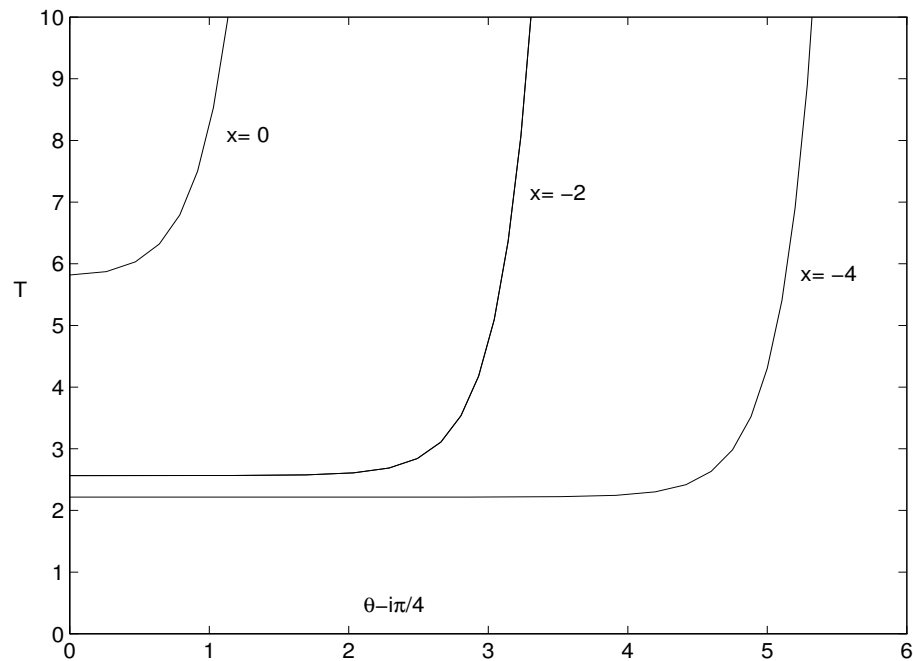


Figure 9: Half-period ( $i\pi/4$ ) shifted  $T(\theta)$  at the self-dual point  $b^2 = 1$ .

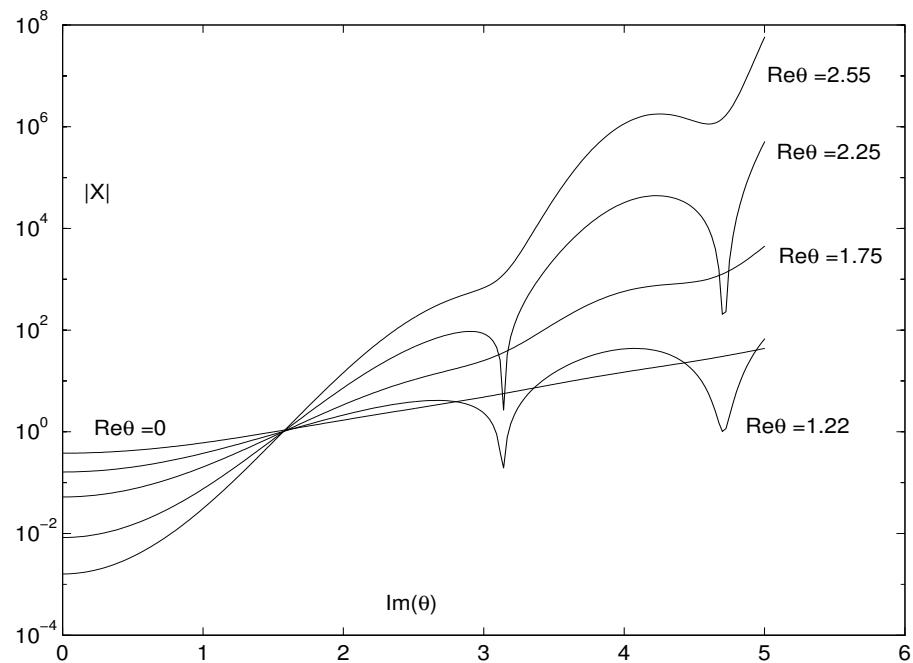


Figure 10:  $|X(\theta)|$  as a function of  $\text{Im } \theta$  at different values of  $\text{Re } \theta$  ( $b^2 = 1$  and  $x = 0$ ).

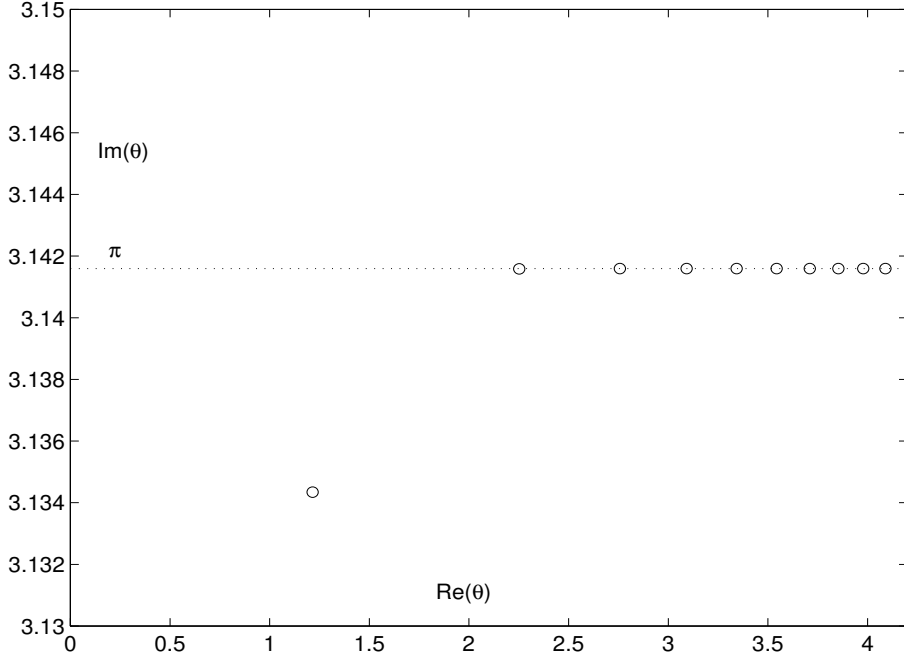


Figure 11: First 10 zeros of  $X(\theta)$  located near the line  $\text{Im } \theta = \pi$ . An example for  $x = 0$  and  $b^2 = 1$ .

close to the positions of the first two zeros of  $T(\theta)$  on the real axis. The deeps near  $\text{Im } \theta = \pi$  and  $\text{Im } \theta = 3\pi/2$  indicate a presence of zeros of  $X(\theta)$  nearby.

More precise positions of zeros of  $X(\theta)$  near the line  $\text{Im } \theta = \pi$  (for the same value  $x = 0$ ) are exemplified in fig.11. In fact all these zeros are inside the strip  $|\text{Im } \theta| < \pi$ . Only the first zero deviates noticeably from the line  $\text{Im } \theta = \pi$ . The imaginary parts of next zeros are already very close to  $\pi$  and tend to this value very fast.

**2. Rational points.** As an example of a rational point we take the simplest case  $b^2 = 1/2$ . The periods of  $T(\theta)$  and  $\tilde{T}(\theta)$  are commensurable and equal to  $2i\pi/3$  and  $i\pi/3$  respectively. In fact in this case there is no need to study separately  $T$  and  $\tilde{T}$  since, as it is readily derived from (2.13), they are bound up by the relation

$$\tilde{T}(\theta) = T(\theta)T(\theta + i\pi/3) - 2 \quad (7.1)$$

It should be noted that similar finite degree functional relations between  $T$  and  $\tilde{T}$  exist for any rational  $b^2$ . For example, at  $b^2 = 1/3$  the periods of  $T$  and  $\tilde{T}$  are  $3i\pi/4$  and  $i\pi/4$  respectively and

$$\tilde{T}(\theta) = T(\theta)T(\theta + i\pi/4)T(\theta + i\pi/2) - T(\theta) - T(\theta + i\pi/4) - T(\theta + i\pi/2) \quad (7.2)$$

Numerical patterns of  $T(\theta)$ ,  $\tilde{T}(\theta)$  and  $X(\theta)$  are essentially the same as for  $b^2 = 1$ . I'd only show few plots of  $|X(\theta)|$  in the complex plane along the lines  $\text{Im } \theta = \pi, 4\pi/3, 5\pi/3, 2\pi, 7\pi/3$

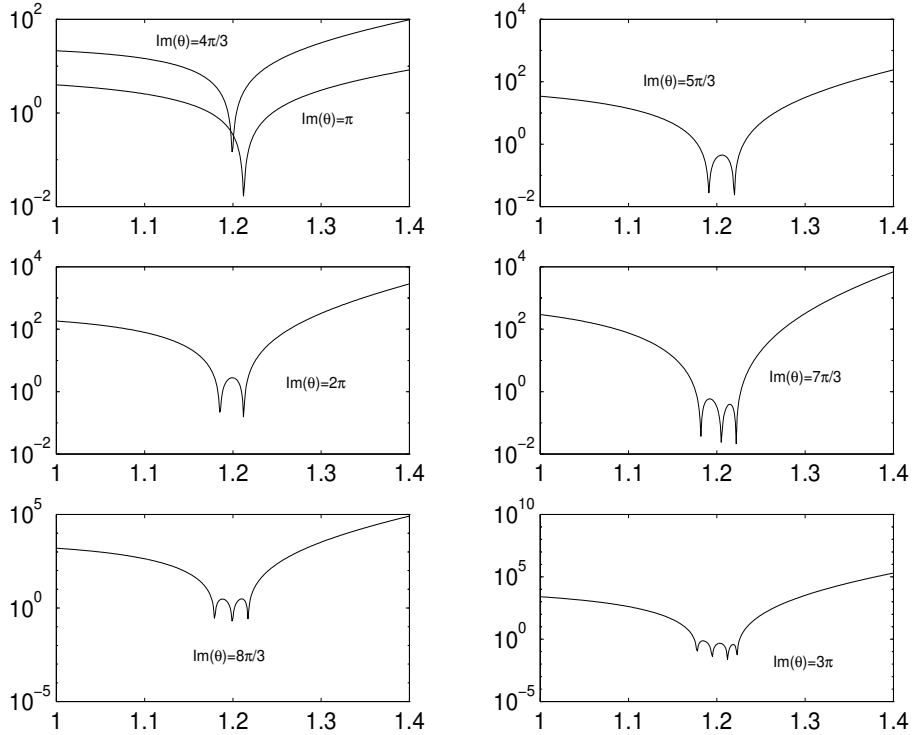


Figure 12:  $|X(\theta)|$  vs.  $\text{Re } \theta$  in the vicinity of the first (multi-)zero at  $\text{Re } \theta \approx 1.2$  and different  $\text{Im } \theta$  ( $x = 0$ ,  $b^2 = 1/2$ ).

etc. to illustrate the mechanism of multiplication of the zeros density in the asymptotics  $\text{Re } \theta \rightarrow \infty$  as required by the prediction of fig.2. In fig.12  $|X(\theta)|$  is plotted at  $\text{Re } \theta$  in the vicinity of the real position of the first zero in  $T(\theta)$  at  $\theta = 1.2241\dots$  (the case  $x = 0$  is taken as an example). At  $\text{Im } \theta = \pi$  and  $4\pi/3$  the picture indicates simple zeros located closely to this point in  $\text{Re } \theta$  and slightly displaced in the imaginary direction. At  $\text{Im } \theta = 5\pi/3$  and  $2\pi$  the zeros are splitted in two closely located ones again near the same position in the real direction. For  $\text{Im } \theta = 7\pi/3$  and  $8\pi/3$  there are triplets of close zeros, etc. In fig.13 the same is exemplified near the next zero of  $T(\theta)$  at  $\theta = 2.2527\dots$ . It is seen already that the scale of splitting becomes very small with  $\text{Re } \theta$  growing and such zero multiplets look like multiple zeros if the numerical resolution is not enough.

**3. General real  $b^2$ .** In general the periods of  $T(\theta)$  and  $\tilde{T}(\theta)$  are incommensurable. As it was mentioned in sect.5, it leads in particular to quite complicated  $\text{Re } \theta \rightarrow \infty$  asymptotics at sufficiently large  $\text{Im } \theta$ . While the analytic structure of  $T(\theta)$  and  $\tilde{T}(\theta)$  remains essentially as described above (in particular, I verified for many examples that all zeroes of  $T$  and  $\tilde{T}$  are on the real axis), the structure of zeros in  $X(\theta)$  becomes, as  $\text{Im } \theta$  comes essentially large, rather chaotic. I hope to turn again to this point in future studies. Let me mention only the following observation concerning the small  $R$  (or large negative  $x$ ) picture. If  $-x \gg 1$ , in the

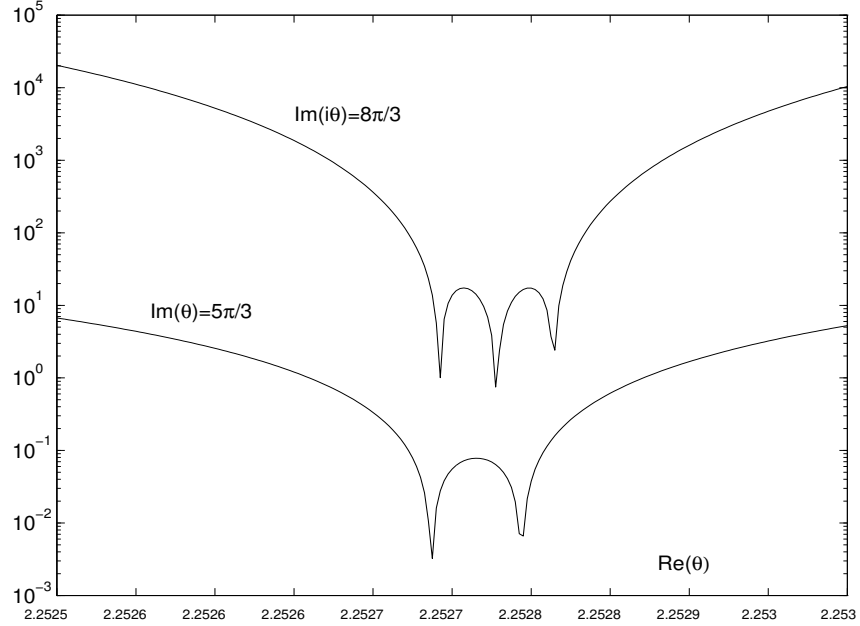


Figure 13: The same as in fig.12 near the next multi-zero at  $\text{Re } \theta \approx 2.2527 \dots$ .

central region  $x < \theta < -x$  function  $X(\theta)$  matches extremely well the following expression

$$X(\theta) = \frac{\cos(2QP\theta)}{[\sinh(2\pi bP) \sinh(2\pi P/b)]^{1/2}} \quad (7.3)$$

where  $P$  is an  $R$ -dependent parameter. Roughly it can be estimated from the requirement that  $X(\theta) \simeq 0$  at  $\theta = \pm x$ , i.e.,  $P = \pi/(-4Qx) + O(x^{-2})$ . Notice that substituting of this approximation to the expression of the effective central charge

$$c_{\text{eff}} = 1 - 24P^2 \quad (7.4)$$

(see ref. [16] for the motivations) we arrive just at the leading UV logarithmic correction (2.16). It is easy to verify that expression (7.3) *satisfies exactly* the functional  $X$ -system (2.13). This means in particular that it remains a valid approximation (at large  $-x$ ) of  $X(\theta)$  in the whole complex strip  $x < \text{Re } \theta < -x$ .

In fact along the lines of [16] and [17] a far better estimate of  $P$  can be found which takes into account all logarithmic in  $R$  corrections to (2.16). In this framework  $P$  is determined as the first root of the transcendental equation

$$4QP \log(R/2\pi) + i \log(-S_L(P)) = -\pi \quad (7.5)$$

where  $S_L(P)$  is the so-called Liouville reflection amplitude (for the arguments see [16])

$$S_L(P) = - \left( \pi \mu \frac{\Gamma(b^2)}{\Gamma(1-b^2)} \right)^{-2iP/b} \frac{\Gamma(1+2ibP)\Gamma(1+2iP/b)}{\Gamma(1-2ibP)\Gamma(1-2iP/b)} \quad (7.6)$$

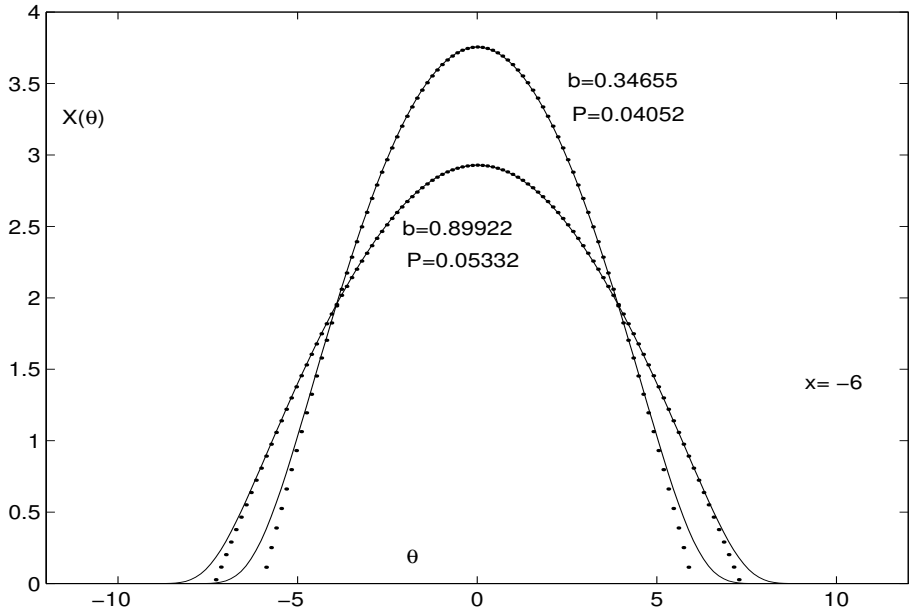


Figure 14: Function  $X(\theta)$  at  $x = -6$  and different values of  $b^2$  (solid lines) compared with the approximation (7.3). Corresponding values of  $P$  are indicated.

For example, in fig.14 the shape of  $X(\theta)$  is compared with the approximation (7.3) for  $x = -6$  and two values of the parameter  $b^2 = 0.8086\dots$  and  $b^2 = 0.1201\dots$  According to (7.6) they correspond to  $P = 0.05332\dots$  and  $P = 0.04052\dots$  respectively.

In view of (7.3) the plateau heights of  $T(\theta)$  and  $\tilde{T}(\theta)$  in the central region  $x < \theta < -x$  and  $x \rightarrow -\infty$  can be estimated as

$$\begin{aligned} T_0 &= 2 \cosh(2\pi b P) \\ \tilde{T}_0 &= 2 \cosh(2\pi P/b) \end{aligned} \tag{7.7}$$

with the same  $P$  determined by (7.6).

**4. Complex (staircase) values of  $b^2$ .** The staircase version of TBA equation (2.3) (with the kernel (6.3)) is solved numerically in the same way as in the ShG case. The structure of the solution has some interesting differences from the case of real  $b$ . The peculiarities are more manifested if parameter  $\theta_0$  in (6.3) is taken sufficiently large and the deep UV region  $-x \gg 1$  is considered.. At  $\theta_0 \gg 1$  parameter  $b$  is close to imaginary unity and

$$Q = \frac{\pi}{\sqrt{\theta_0^2 + \pi^2/4}} \tag{7.8}$$

is small.

In fig.15 two pictures of  $X(\theta)$  on the real axis are plotted for  $x = -46$  and  $x = -91$ , both at  $\theta_0 = 20$ . The characteristic staircase behavior (in fact very similar to that of

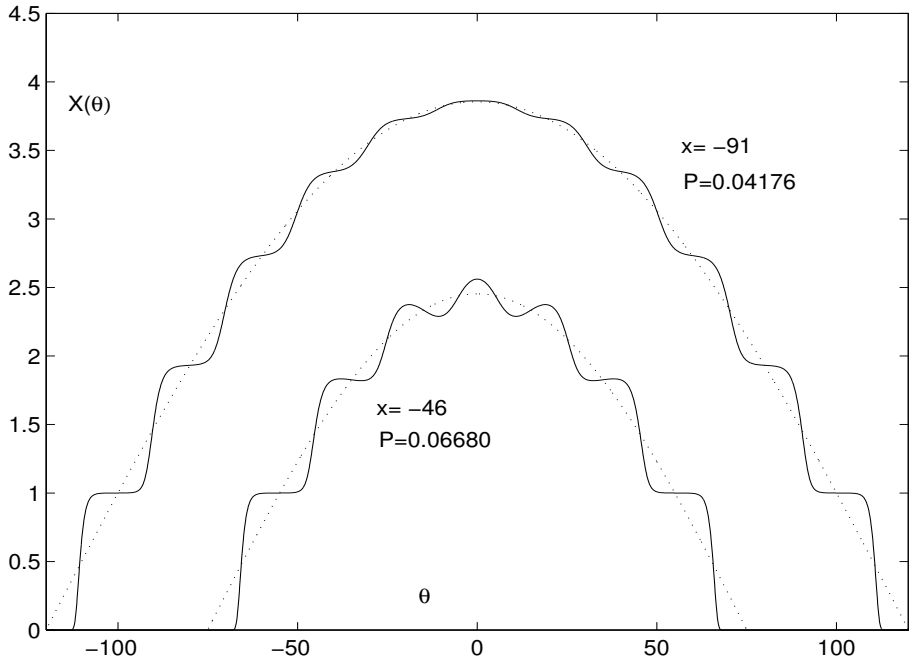


Figure 15: Staircase function  $X(\theta)$  at real  $\theta$  compared with the approximation (7.3) ( $\theta_0 = 20$ ).

$Y(\theta)$  observed in ref. [10]) is very apparent. It is seen also that expression (7.3) with the parameter  $P$  determined as the solution to the staircase version of (7.5) (in the present case  $P = 0.06680\dots$  and  $P = 0.04176\dots$  respectively) still follows in the central region the average behavior of the solution. The deviations (or in other words the corrections to the approximation (7.3)) are now oscillating and much bigger then in the ShG case. At sufficiently large  $-x$  (many amounts of  $\theta_0$ ) the ascending part (starting from  $\theta = x - \theta_0$ ) of the staircase consists of a succession of almost flat steps of constant width  $\theta_0$ , the heights being very well fitted by the expression

$$X_n = \frac{\sin(2QPn/\theta_0)}{\sin(2QP/\theta_0)} \quad (7.9)$$

with  $n = 0, 1, 2, \dots$ . It should be noted that for the reasons to be explained just below, in the case of complex  $b$  expression (7.3) does not give an approximation in the whole strip  $x < \operatorname{Re} \theta < -x$ . Although (7.3) is still an exact solution to the staircase  $X$ -system (6.6), its validity is restricted to a certain parallelogram in the complex  $\theta$ -plane.

To see this in fig.16 I present the location of zeros of the function  $X(\theta)$  (at  $\theta_0 = 20$  and  $x = -46$ ) in the upper half-plane. The picture is obviously reflected to the lower half-plane by the symmetry of  $X(\theta)$ . We see several strings of zeros accumulating along the lines  $\operatorname{Im} \theta = \pi n/2$ ,  $n = 2, 3, 4, \dots$  which start at the values  $\operatorname{Re} \theta_2 = 47.1500\dots$ ,  $\operatorname{Re} \theta_3 = 27.12267\dots \approx \operatorname{Re} \theta_2 - \theta_0$ ,  $\operatorname{Re} \theta_4 = 7.11742\dots \approx \operatorname{Re} \theta_3 - \theta_0$  etc. There are opposite sets of

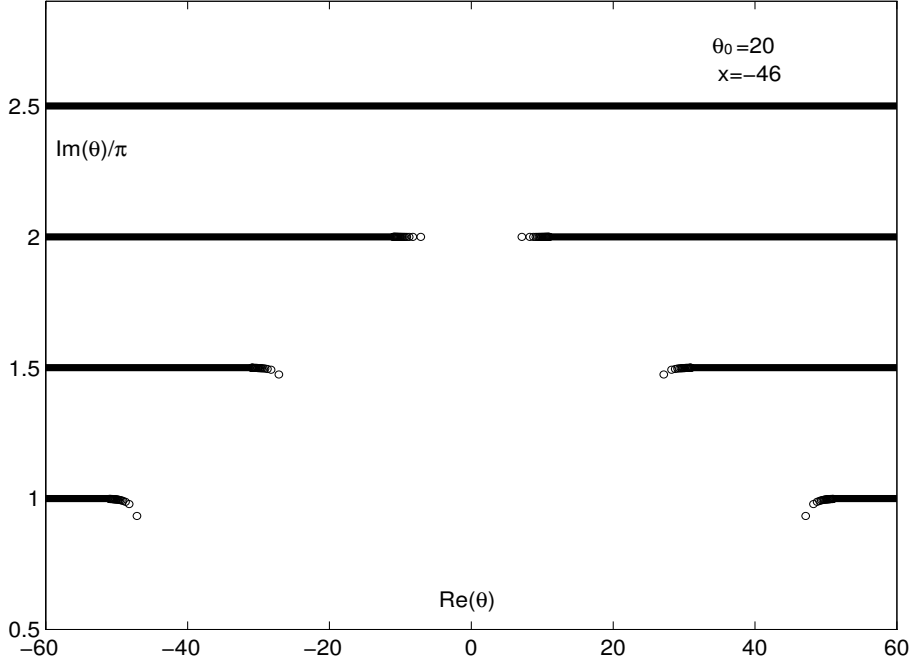


Figure 16: Zeros of  $X(\theta)$  at  $\theta_0 = 20$  and  $x = -46$ . Solid lines stand for very dense sets of zeros.

strings symmetric with respect of the imaginary axis. As  $n$  grows they are shifted in steps of  $-\theta_0$  and  $\theta_0$  respectively and meet each other at a certain value of  $n$  ( $n = 5$  in the present example). After that, continuous lines of dense zeroes extending from  $-\infty$  to  $\infty$  are formed. In general at large  $\theta_0$  the first such line is already dense enough to produce the effect of a “cut” where the behavior of  $X(\theta)$  changes drastically. In our example, across the first “cut” at  $\text{Im } \theta = 5\pi/2$  the absolute value of  $X(\theta)$  jumps by many ( $10^5$ ) orders of magnitude. This is exemplified in fig.17 where  $X(\theta)$  is plotted along the imaginary axis. Notice that before  $\text{Im } \theta = 5\pi/2$  function  $X(\theta)$  is almost constant. As  $\theta_0$  grows this effect becomes more and more dramatic and in the limit  $\theta_0 \rightarrow \infty$  the lines of zeros become real cuts. In the forthcoming paper [18] I’m going to comment more on this effect which plays a crucial role in the analytic connection between the staircase behavior at finite  $\theta_0$  and the “sin-Gordon” solutions corresponding to purely imaginary  $b = i\beta$ .

In fig.18 location of zeros of the periodic function  $T(\theta)$  is shown at the “moderate” value  $\theta_0 = 1$  and different  $x$ . The picture is presented here just to demonstrate two observations: (a) At staircase values of  $b$  zeros of  $T(\theta)$  are not exactly on the real axis but displaced slightly to the complex plane, the displacement becoming negligible very quickly with the number of zero. (b) At  $x \rightarrow -\infty$  the picture of zeros is “frozen” in the sense that at  $x$  sufficiently large the pattern of zeros is simply shifted by the amount  $\Delta x$  in the  $\theta$  plane as one changes  $x \rightarrow x - \Delta x$ . As it is usual in the TBA practice, it is convenient to study these frozen limiting patterns substituting the original “massive” TBA equation (2.3) by the massless

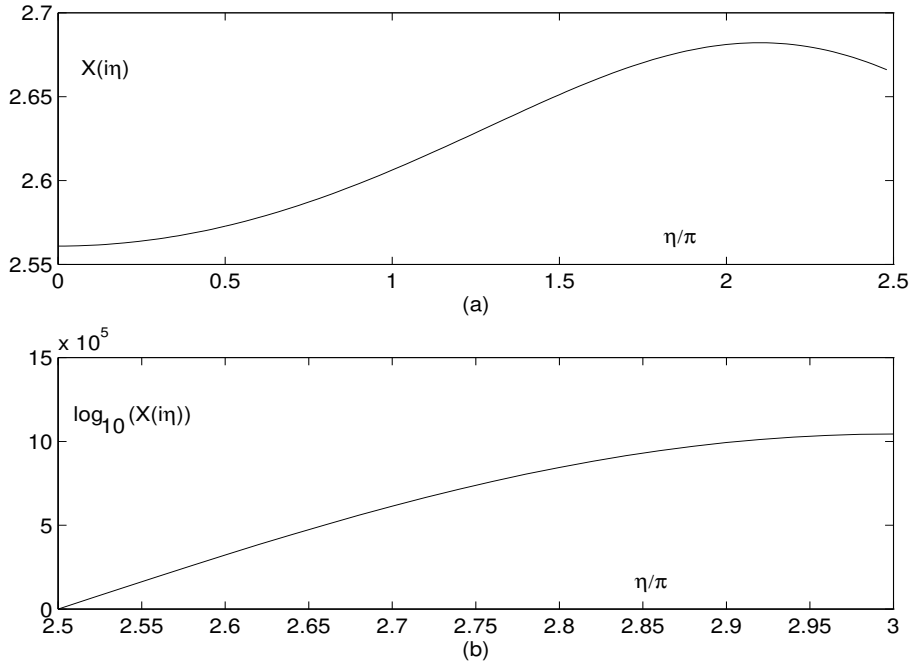


Figure 17:  $X(\theta)$  along the imaginary axis ( $\theta_0 = 20$ ,  $x = -46$ ). Plot (b) is in the decilogarithmic scale.

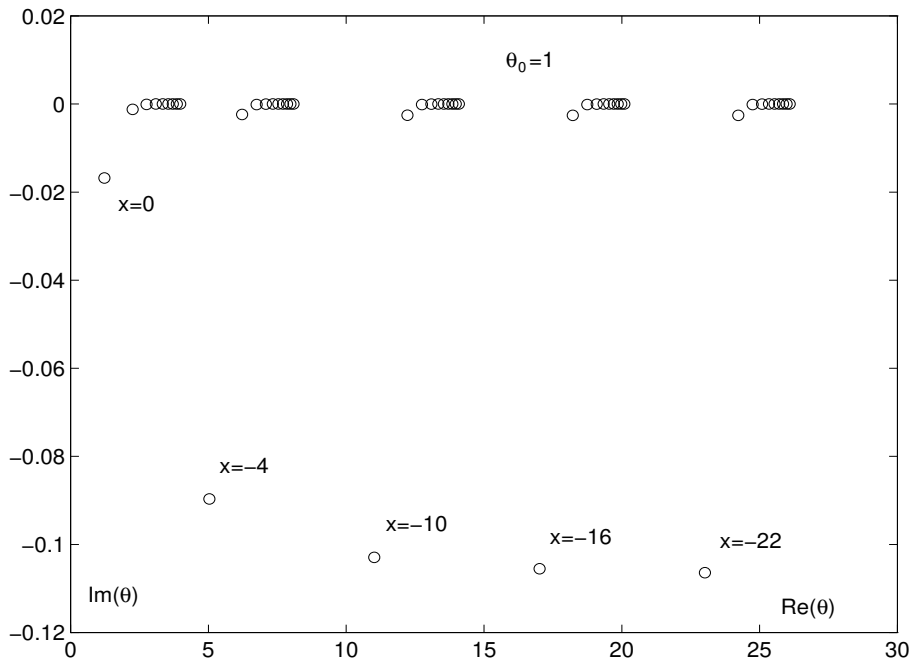


Figure 18: Zeros of  $T(\theta)$  at  $\theta_0 = 1$  and different  $x$ .

version of it. This is one of the motivations for the subsequent study (to be published [18]).

## 8. Concluding remarks

- In the present study I didn't touch at all the important question about the  $R$  (or  $x$ ) dependence of the effective central charge (2.2) determined through the finite-size ground state energy (2.1). The UV behavior at  $x \rightarrow -\infty$  is especially interesting since the analytic structure of  $c_{\text{eff}}(R)$  is quite unusual (like in (2.16)). The Liouville quantization condition (7.5) together with (7.4) proves to be a very good approximation to the UV effective central charge behavior. However, while it takes into account all the “soft” (logarithmic in  $R$ ) contributions to the asymptotic, there are certainly power-like corrections in  $R$ . The most important of them (at least at real  $b$ ) is the contribution of the ground state energy (1.9). Approximation (7.4) is essentially improved if it is taken into account

$$c_{\text{eff}} = 1 - 24P^2 + 3(mR)^2/(4\pi \sin \pi p) \quad (8.1)$$

Usually after the ground state energy contribution is subtracted the remainder is a series in the perturbative powers of  $R$  like in (2.15). In our present case with Lagrangian (1.1) naively one could expect a series like

$$c_{\text{eff}} - 3(mR)^2/(4\pi \sin \pi p) = 1 - 24P^2 + \sum_{n=1}^{\infty} c_n(P) \left( \mu R^{2+2b^2} \right)^{2n} \quad (8.2)$$

where the powers of  $R$  are predicted on the dimensional arguments and the coefficients  $c_n(P)$  are something like the Coulomb gas perturbative integrals corresponding to expansion in  $\mu$  around the vacuum of momentum  $P$  (therefore they keep some smooth  $R$  dependence). Although the leading correction  $n = 1$  of order  $R^{4+4b^2}$  is likely in agreement with the numerical data (at least at sufficiently small  $b^2$ ), the whole structure (8.2) certainly contradicts duality. Correct expansion must contain also the “dual” corrections with powers  $R^{4+4/b^2}$ . Of course many people immediately propose to add the dual interaction to the Lagrangian and consider an action like

$$A_{\text{trivial}} = \int \left[ \frac{1}{4\pi} (\partial_a \phi)^2 + 2\mu \cosh(2b\phi) + 2\tilde{\mu} \cosh(2b^{-1}\phi) \right] d^2 x \quad (8.3)$$

with  $\tilde{\mu}$  taken from (1.8) or sometimes introduced as an independent coupling. Simultaneous expansion in both couplings would supposedly lead to a self-dual series

$$c_{\text{eff}} - 3(mR)^2/(4\pi \sin \pi p) = 1 - 24P^2 + \sum_{m,n=1}^{\infty} c_{m,n}(P) \mu^{2m} \tilde{\mu}^{2n} R^{4Q(mb+n/b)} \quad (8.4)$$

Coefficients  $c_{m,n}(P)$  are computed as the mixed Coulomb gas integrals which include both kinds of charges produced by the expansion of action (8.3). Although the general

structure of (8.4) looks very likely, to my sense this scenario (which I call trivial) with naive addition of dual interactions (as in (8.3)) is not exactly in the spirit of duality. However at present it does not contradict any data and in fact should be verified. A check of this trivial scenario (as well as any other one) requires very subtle measurements of the subleading power-like corrections to the effective central charge as well as tedious calculations of mixed perturbative integrals. I understand that this is a *quantitative* work which hardly can be replaced by general speculations.

- Of course the definition of  $P$  as the solution to the quantization condition (7.5) is not completely unambiguous. The power-like in  $R$  corrections (which are exponentially small in  $1/P$ ) can be arbitrarily redistributed between the expression for the observable effective central charge (8.4) and the formulation of the quantization condition. In other words one can add exponentially small in  $1/P$  corrections to (7.6) and consider this as a new definition of  $P$ . The problem is that at present the parameter  $P$  is not precisely observable, i.e., it cannot be directly measured in the TBA calculations (apart from the abovementioned *definition* through the observable finite-size effective central charge).
- At this point we arrive at the most intriguing question touched only slightly in the present study. This is about the possibility to construct the solutions  $Q_{\pm}(\theta)$  and  $\tilde{Q}_{\pm}(\theta)$  of eqs.(4.11) with the properties (4.12) and (4.13) such that the solution to (2.3) can be built as the combination (4.14). Was this be possible we'd have another unambiguous definition of the parameter  $P$  as the Floquet index in (4.12). However, there are serious doubts that such solutions exist in any sense, at least for rational values of  $b^2$ . To clarify this point, in the next publication [18] I'll consider the massless version of the ShG TBA equation where the parameter  $P$  is introduced from the very beginning instead of the scale parameter  $R$ . In this context the solutions (4.12) can be found at least as formal series for irrational values of  $b^2$  in the way that the construction (4.14) can be given an exact sense.
- In connection with the periodic structures encoded in the functions  $T(\theta)$  and  $\tilde{T}(\theta)$ , it seems quite interesting to understand better the  $R$  dependence of the coefficients  $T_n$  and  $\tilde{T}_n$  in the expansions (4.9) or (6.9). I checked numerically the  $R \rightarrow 0$  asymptotic of  $T_0$  and  $\tilde{T}_0$ . The leading asymptotics of  $T_0$  and  $\tilde{T}_0$  (remember that for definiteness in this study I always take  $b \leq 1$ , in particular the data discussed in this item were calculated at  $b = 0.3466$ ) are very well fitted by the expressions (7.7) with  $P$  the solution to (7.5). The correction to (7.7) for  $T_0$  can be set in the form

$$T_0 = 2 \cosh(2\pi b P) + (mR/2\pi)^{4bQ} T_0^{(1)}(P) \quad (8.5)$$

where  $T_0^{(1)}(P)$  is a smoothly varying function of  $P$  with certain UV limit  $T_0^{(1)}(0)$ . As for  $\tilde{T}_0$  the correction is better fitted as

$$\tilde{T}_0 - 2 \cosh(2\pi P/b) \sim A(P)(mR/2\pi)^{\alpha} \quad (8.6)$$

with  $\alpha$  again numerically close to  $4bQ$ . The common TBA experience would expect from the periodic structure of  $\tilde{T}(\theta)$  a much smaller correction  $\sim (mR/2\pi)^{4Q/b}$ . A probable explanation is that there are some power-like corrections to the Liouville quantization condition (7.5) so that the “correct” value of  $P_{\text{correct}}$  is off from  $P$  (calculated from (7.5)) by an amount of order  $(mR/2\pi)^{4bQ}$

$$P = P_{\text{correct}} + P_{1,0}(mR/2\pi)^{4bQ} + \dots \quad (8.7)$$

With this  $P_{\text{correct}}$  an asymptotic

$$\tilde{T}_0 = 2 \cosh(2\pi P_{\text{correct}}/b) + (mR/2\pi)^{4Q/b} \tilde{T}_0^{(1)}(P_{\text{correct}}) + \dots \quad (8.8)$$

must hold. If the power  $4Q/b \gg 4bQ$  (like in the present experiment with  $4Q/b = 37.31\dots \gg 4bQ = 4.480\dots$ ) we can even try to relate the coefficient  $A$  in (8.6) to the leading power correction to (7.5). As the corrections in (8.8) are much more suppressed at  $R \rightarrow 0$  this seems reasonable.

- It is easy to verify that the leading asymptotic of the higher coefficients  $T_n$  and  $\tilde{T}_n$  in the expansion (4.9) are of the form

$$\begin{aligned} T_n &= (mR/2\pi)^{2bQ|n|} T_n^{(0)}(P) + \dots \\ \tilde{T}_n &= (mR/2\pi)^{2Q|n|/b} \tilde{T}_n^{(0)}(P) + \dots \end{aligned} \quad (8.9)$$

with  $T_n^{(0)}(P)$  and  $\tilde{T}_n^{(0)}(P)$  regular at  $P = 0$ . I analysed quantitatively the functions  $T_1^{(0)}(P)$  and  $\tilde{T}_1^{(0)}(P)$ . Motivated by the constructions of refs. [14, 19] let us introduce slightly rescaled functions

$$\begin{aligned} t_1(P) &= T_1^{(0)}(P) (Z(p))^{-2bQ} \\ \tilde{t}_1(P) &= \tilde{T}_1^{(0)}(P) (Z(p))^{-2Q/b} \end{aligned} \quad (8.10)$$

with  $Z(p)$  defined in (1.7). In table 1 the values of  $t_1(P)$  and  $\tilde{t}_1(P)$  are compared with the following analytic expressions borrowed from refs. [14, 19] where these coefficients enter the explicit constructions of the “sin-Gordon” (i.e., related to purely imaginary values of  $b$ ) analogs of  $T(\theta)$

$$\begin{aligned} t_1^{\text{CFT}}(P) &= -\frac{4\pi^2\Gamma(1+2b^2)}{\Gamma^2(b^2)\Gamma(1+b^2+2iP)\Gamma(1+b^2-2iP)} \\ \tilde{t}_1^{\text{CFT}}(P) &= -\frac{4\pi^2\Gamma(1+2b^{-2})}{\Gamma^2(b^{-2})\Gamma(1+b^{-2}+2iP/b)\Gamma(1+b^{-2}-2iP/b)} \end{aligned} \quad (8.11)$$

The TBA numbers are measured at  $b = 0.3465545\dots$  and different values of  $x$ . The same for the staircase example  $\theta_0 = 10$  is presented in table 2. The convergence is noticeably slower due to much weaker suppression of the higher power corrections ( $\text{Re}(4 + 4b^2) = 0.1926\dots$  in this case). The numbers quoted make it clear that an

$x$	$P$	$t_1^{\text{TBA}}$	$t_1^{\text{CFT}}$	$\tilde{t}_1^{\text{TBA}}$	$\tilde{t}_1^{\text{CFT}}$
0	0.3896985	-0.7228948	-0.7213854	-1.452134e-2	-1.437650e-2
-2	0.1152693	-0.6585087	-0.6585077	-8.578078e-3	-8.578008e-3
-4	6.046935e-2	-0.6542746	-0.6542746	-8.272562e-3	-8.272562e-3

Table 1: Numerical values of

$x$	$P$	$t_1^{\text{TBA}}$	$t_1^{\text{CFT}}$
0	0.1771863	0.0711632-1.1669319i	0.0051770-1.1896763i
-15	8.604775e-2	-0.0660054-0.7447625i	-0.0684458-0.7445886i
-30	5.695833e-2	-0.0708064-0.6568688i	-0.0709316-0.6568002i

Table 2: Numerical values of

analytic continuation of the constructions of refs. [14,19] for the ShG or staircase values of the parameter is quite relevant. The corresponding “CFT integrable structures” will be shown to have a precise relation to the solutions of the massless versions of ShG and staircase TBA equations [18] where the parameter  $P = P_{\text{correct}}$  is fixed by construction.

- I’d like to mention a quite intriguing recent article [20] where the author arrived at the function (2.9) in a rather different context. It appears as the exact wave function of the finite-size sinh-Gordon model in special “ $\gamma$ -coordinates” which are the sinh-Gordon version of the Flaschka-McLaughlin variables (see [20] for the details). This gives again a motivation to continue the study of the analytic structures related to the ShG TBA equation.

**Acknowledgments.** I acknowledge very useful discussions with C.Ahn, V.Bazhanov, V.Fateev, C.Rim and mostly with A.Zamolodchikov. I thank also P.Wiegmann who brought my attention to papers [12,13] and introduced to me the world of incommensurable periods. Discussions with G.Mussardo about the “double sin-Gordon” [21] were also quite relevant. My special gratitude is to S.Lukyanov who communicated me his article [20] before publication and encouraged my work by exciting discussions.

The work is supported in part by EU under the contract ERBFMRX CT 960012.

## References

- [1] S.Vergeles and V.Gryanik. *Yad.Fiz.* 23 (1976) 1324.
- [2] I.Arefyeva and V.Korepin. *JETP Letters*, 20 (1974) 680.
- [3] Al.Zamolodchikov. Mass scale in sin-Gordon and its reductions. *Int.J.Mod.Phys.* A10 (1995) 1125.
- [4] C.Deatri and H.deVega. *Nucl.Phys.* B358 (1991) 251.

- [5] S.Lukyanov and A.Zamolodchikov. Exact expectation values of local fields in quantum sine-Gordon model. *Nucl.Phys.* B493 (1997) 571.
- [6] V.Fateev, D.Fradkin, S.Lukyanov, A.Zamolodchikov and Al.Zamolodchikov. Expectation values of descendent fields in the sine-Gordon model. *Nucl.Phys.* B540 (1999) 587.
- [7] A.Koubek and G.Mussardo. On the operator content of the sinh-Gordon model. *Phys.Lett.* B311 (1993) 193.
- [8] Al.Zamolodchikov. *Phys.Lett.* B253 (1991) 391.
- [9] E.Quattrini, F.Ravanini and R.Tateo. Integrable QFT(2) encoded in products of Dynkin diagrams. Bologna-preprint DFUB-93-11 (hep-th/9311116).
- [10] Al.Zamolodchikov. Resonance factorized scattering and roaming trajectories. ENS-LPS-335, 1991, unpublished.
- [11] R.Hirota. *J.Phys.Soc.Japan*, 50 (1981) 3785.
- [12] P.Wiegmann. Bethe ansatz and classical Hirota equations. *Int.J.Mod.Phys.B* 11 (1997) 75 (cond-mat/9610132).
- [13] P.Wiegmann and A.Zabrodin. Algebraization of difference eigenvalue equations related to  $U_q(sl_2)$ . (cond-mat/9501129).
- [14] V.Bazhanov, S.Lukyanov and A.Zamolodchikov. Integrable structure of conformal field theory II. Q-operator and DDV equation. *Commun.Math.Phys.* 190 (1997) 247.
- [15] R.Hirota. *J.Phys.Soc.Japan*, 56 (1987) 4285.
- [16] A.Zamolodchikov and Al.Zamolodchikov. Structure constants and conformal bootstrap in Liouville field theory. *Nucl.Phys.* B477 (1996) 577.
- [17] C.Ahn, V.Fateev, C.Kim, C.Rim and B.Yang. Reflection amplitudes of ADE Toda theories and thermodynamic Bethe ansatz. *Nucl.Phys.* B656 (2000) 210.
- [18] Al.Zamolodchikov. Massless sinh-Gordon TBA equations, in preparation.
- [19] V.Bazhanov, S.Lukyanov and A.Zamolodchikov. Integrable structure of conformal field theory, quantum KdV theory and thermodynamic Bethe ansatz. *Commun.Math.Phys.* 177 (1996) 381.
- [20] S.Lukyanov. Finite Temperature Expectation Values of Local Fields in the sinh-Gordon Model. RUNHETS-2000-17.
- [21] G.Delfino and G.Mussardo. Non-integrable aspects of the multi-frequency sine-Gordon model. *Nucl.Phys.* B516 (1998) 675.